

4 Stable, static Curvature-cosmology

5 DAVID F.CRAWFORD¹

6 ¹*School of Physics (Retired), University of Sydney, NSW, 2006, Australia*

7 (Dated: July 20, 2022)

8 ABSTRACT

9 This paper describes Curvature-cosmology that is a tired-light cosmology that predicts a well-defined
10 static and stable universe. It provides a new simpler raw data analysis for Type Ia supernova. Since
11 it is a complete challenge to the big bang paradigm, Curvature-cosmology can only be judged by
12 its agreement with direct cosmological observations. Curvature-cosmology predicts a universe of a
13 hydrogen plasma with a temperature of 2.456×10^9 K [observed: 2.62×10^9 K] and a cosmic background
14 radiation temperature of 2.736 K [observed: 2.725K]. It has only one parameter which is the density
15 of the cosmic plasma. The major observations that are shown to consistent with it are: Type Ia
16 supernova, Tolman surface brightness, angular size, galaxy distributions, X-ray background radiation,
17 and quasar variability. It does not need inflation, dark matter or dark energy.

18 *Keywords:* cosmology, supernova

19	Contents	40	4. Part C: Observations	15
20	1. Introduction	2	4.1. Type Ia supernova	15
21	2. Part A: Analysis of Type Ia Supernova	2	4.2. X-ray background radiation	15
22	2.1. Introduction	2	4.3. Cosmic microwave background radiation.	17
23	2.2. Type Ia supernova	3	4.4. Tolman surface .	18
24	2.3. The observations.	4	4.5. Dark matter and Coma cluster	20
25	2.4. Results for the light curve width	4	4.6. Angular size	22
26	2.5. Supernova absolute magnitudes.	6	4.7. Galaxy distribution	23
27	2.6. Discussion of SALT2 supernova	7	4.8. Quasar variability in time	23
28	magnitudes.	7	4.9. The Butcher-Oemler effect	24
29	3. Part B: Curvature-cosmology theory.	7	4.10. Fluctuations in the CMBR	24
30	3.1. Introduction	7	4.11. Pioneer 10 acceleration.	24
31	3.2. Derivation of Curvature-redshift	8	4.12. The Sunyaev–Zel’dovich effect	26
32	3.3. Gravitation is not a force	9	4.13. Gravitational lensing.	26
33	3.4. Derivation of Curvature-pressure.	10	4.14. Lyman_alpha forest	26
34	3.5. The Curvature-cosmological model	11	4.15. Nuclear abundances	28
35	3.6. Distance modulus.	12	4.16. Galactic rotation curves	28
36	3.7. Temperature of the cosmic plasma	13	4.17. Redshifts in our Galaxy	28
37	3.8. Black holes and Jets	13	4.18. Anomalous redshifts	29
38	3.9. Inhibition of Curvature-redshift	13	4.19. Voids	29
39	3.10. Possible laboratory tests.	14	4.20. Entropy	30
			4.21. Olber’s Paradox	31
			4.22. Philip’s relation	31
		63	5. Conclusions	31
		64	6. Author biography	32

1. INTRODUCTION

Nearby Type Ia supernovae are well known to have essentially identical light curves that make excellent cosmological probes. The observational evidence for their time dilation has a long history with notable papers being by Goldhaber et al. (2001, 1996); Blondin et al. (2008). More recent contributions are by Kowalski et al. (2008); Wood-Vasey et al. (2008); Kessler et al. (2009a); Amanullah et al. (2010); Conley et al. (2011); Betoule et al. (2014); Scolnic et al. (2018). All of these recent papers use the SALT2 Guy et al. (2010, 2007) method to determine the widths and peak flux densities of the supernova and they have used the Λ CDM expansion cosmology to determine absolute magnitudes.

These papers show that type Ia supernova observations provide the major contribution to cosmological models.

A crucial property of Curvature-cosmology is that the observed magnitude is the sum of an intrinsic magnitude, which is what would be observed by a nearby observer and a cosmological magnitude. The cosmological magnitude is a comes from the change in the average energy of the photons due to their trajectory through the universe. Whereas the intrinsic magnitude is only a property of the observed object and is completely independent of the cosmology.

This paper has three major parts where the first part presents a new much simpler method that analyzes raw Type Ia supernova data in order to produce their light curve widths and their peak flux densities. These results are compared with the standard SALT2 method and it showed that the SALT2 method (summarized in the appendix) has a flaw in its flux density results.

The second part presents a new static cosmology, Curvature-cosmology, that has excellent agreement with observations.

The third part provides the observation data for all major cosmological observations and discusses the results in the context of Curvature-cosmology.

It is followed in section 5 by a summary of the quantitative observations that are relevant to Curvature-cosmology.

The common attribute of all Λ CDM , cosmologies is that they are based on the assumption that the universe is expanding (Peebles 1993). An early alternative was the steady-state theory of Hoyle, Bondi and Gold Hoyle (1962) (described with later extensions by Hoyle et al. (2000)) that required continuous creation of matter. However steady-state theories have serious difficulties in explaining the cosmic microwave background radiation. This left Λ CDM as the dominant cosmology but still subject to criticism.

Lal (2010) and Joseph (2010) have continued major earlier criticisms of Λ CDM cosmologies (Ellis 1984; Lerner 1991; Disney 2000; van Flandern 1991). Whereas most of these criticisms have been of a theoretical nature, this paper concentrates on whether observational data supports a static cosmological model, Curvature-cosmology, described below.

The purpose of this paper is to examine all major cosmological observations and to show that with minor exceptions they are in agreement with a this static model.

This paper is the culmination of many years of work and is a complete re-synthesis of many approaches that I have already published (Crawford 1987a,b, 1991, 1993, 1995a,b, 1998, 1999a,b, 2006, 2009a,b). These papers are cited to show the convoluted and historical path of Curvature-cosmology. Because hypotheses and notations have changed and evolved, direct references to these earlier versions of the theory would be misleading and all relevant results are published in this paper.

For convenience it is assumed that the wavelength dependence of a band can be replaced by a single value, λ , which is the mean wavelength for that band.

2. PART A: ANALYSIS OF TYPE IA SUPERNOVA

2.1. Introduction

This part describes a new analysis method (intrinsic analysis) for Type Ia supernova that is simple and can replace the standard SALT2 method. A major difference from SALT2 is that it explicitly estimates and uses intrinsic flux densities. Its use in an analysis of 1,707 light curves for Type Ia supernova provides a width regression,

$$w_{obs}(z) = 1.060 \pm 0.009 + (1.080 \pm 0.042)z, \quad (1)$$

which is in excellent agreement with a $(1+z)$ dependence and justifies the analysis method. An analysis of 635,218 quasar observations shows that their flux density is proportional to $-(1+z)(1.0073 \pm 0.0046)$ which verifies a universal energy $(1+z)$ dependence.

It is shown that absolute magnitudes of Type Ia supernova analyzed with the SALT2 method and using the Λ CDM distance modulus are independent of redshift. However supernova analyzed with the intrinsic analysis and using the Λ CDM distance modulus have a significant dependence on redshift which implies a fault in the SALT2 analysis .

Although the intrinsic magnitude is the same as absolute magnitude, the different name is used because the measurement method is different. The intrinsic magnitude can only be used when there are many bands and relies on the fact that each **band** must have the same

cosmological magnitude. Whereas the absolute magnitude requires a cosmological model for the distance modulus and can be applied to a single observation.

The next section covers the results for intrinsic magnitudes for both Type Ia supernova and quasars. An important product is plots of intrinsic magnitudes versus intrinsic wavelengths, both of which appear to be dominated by atomic hydrogen absorption.

Section 2.5 is about absolute magnitudes. Although the absolute magnitudes for supernova analyzed with the SALT2 method and the λ CDM model show no dependence with redshift. The absolute magnitudes for intrinsic analysis and the λ CDM model are significantly different from zero

Section 2.6 Provides a discussion of why the λ CDM model may be flawed.

2.2. Type Ia supernova

From Wikipedia: “Type Ia Supernova is believed to result from mass accretion to a carbon-oxygen white dwarf in a close binary system. When the white dwarf mass exceeds the Chandrasekhar limit, the degenerate electron pressure can no longer support the accumulated mass and the star collapses in a thermonuclear explosion producing a supernova. The peak luminosity of supernova Ia is set by the radioactive decay chain, and the observed photometric correlation between the peak luminosity and the time-scale over which the light curve decays from its maximum is understood physically as having both the luminosity and opacity being set by the mass of Nickel-56 synthesized in the explosion.”

The major observational evidence for Type Ia supernova is a lack of hydrogen lines and a singly ionized silicon (Si II) absorption feature at $0.615\mu\text{m}$ near peak brightness.

The observation of a distant supernova requires the emission of a photon from an intrinsic source and then it follows a trajectory that is determined by the geometry of the universe. If the universe is expanding then their average energy is determined by velocity of the telescope relative to the source. If the universe is static, this energy loss could be the result of photons being scattered outside the beam.

A critical part in measuring the light curve width of Type Ia supernova light curves is to have a reference light curve. The observed light curve must have the same shape independent of redshift. Only its width and height will vary with redshift. Consequently this property is assumed in intrinsic analysis.

In order to remove any possible bias, a standard independent template, the *B* band Parab-18 from Table 2 from Goldhaber et al. (2001) which has the first half-

peak width at -10.1 days and the second half-peak width at 22.3 days is used. Consequently all widths are relative to this light curve.

The purpose of the light-curve analysis is to obtain estimates of the peak flux density for each band, the width (common to all bands) of the light-curve relative to the template and the epoch offset of the light curve. This offset is a nuisance parameter that allows for the unknown epoch of the peak flux density and is defined to be the epoch difference between the fitted light curve relative to the observed epochs.

An initial problem is to determine the initial epoch offset q . The solution used was to estimate the average flux density for every epoch in the observed range. This averaging used a Gaussian weight factor with the $weight = \exp(-0.5(p_i - q)^2)$ where p_i is the epoch of an observation and q is the reference epoch. The day with the largest average flux density defined the initial epoch offset.

The intrinsic analysis method starts with the observed flux density, f_i for the index i , and its uncertainty σ_i . Then for each supernova and each band the maximum likelihood method is used to determine the fitted maximum flux density, F and its epoch.

Let the reference supernova light curve be referenced by $C((p_i - q)/w)$ where p_i is the epoch, w is the computed width, and q is the epoch offset of the maximum of the fitted light curve. Then, assuming a Gaussian flux density noise distribution, the log-likelihood function for a single band, with n observations, of a supernova is

$$\mathcal{L} = \sum_{i=1}^n \left[\left(\frac{f_i - b - F \times C((p_i - q)/w)}{\sigma_i} \right)^2 \right] \quad (2)$$

where i is the observation index, the epoch is p_i and b is the base flux density level for the current band. A constant term that depends only on the measurement uncertainties is omitted. Additionally the omission of the factor $-1/2$ means that \mathcal{L} is a ψ^2 variate with n degrees of freedom. Thus the maximization of the likelihood is identical to the minimization of \mathcal{L} .

Although the peak flux density and base level are determined by an analytic fit, the values for the epoch offset and width are easily found by numerical minimization. Fortunately, the flux density and width are almost orthogonal so that a sequence of alternate fits rapidly converges.

Note that in Eq 2 each flux density and each peak flux density is divided by its uncertainty which means that the fitted width is independent of individual band calibrations and all bands can be included in the same expression.

264 All the information about the width distribution is
 265 contained in \mathcal{L} . The uncertainty in the width was deter-
 266 mined from the proposition that the likelihood function,
 267 \mathcal{L} as a function of width is equal to the likelihood of a
 268 Gaussian function of width with a standard deviation
 269 equal to the width uncertainty. That is

$$\mathcal{L} = \left(\frac{\Delta w}{\sigma_w}\right)^2, \quad (3)$$

270 where Δw is the width offset and σ_w is the estimated
 271 uncertainty in the width and it is estimated using Eq. 2.

272 It must be noted that the fitting procedure is com-
 273 pletely independent of the redshift and is also indepen-
 274 dent of the band type. Although each band had its own
 275 estimate of its peak flux density, the width is the result
 276 of a common fit to all observations for each supernova.
 277 Thus the computed parameters for each supernova are
 278 its light curve width, and the peak flux density for each
 279 band which is the flux density for that band at the max-
 280 imum epoch of the common fitted light curve.

281 2.3. The observations.

282 The Type Ia supernova data used here comes from
 283 the Supernova Legacy survey (SNSL), the Sloan Digital
 284 Survey (SDSS) (both sourced from the SNANA website
 285 Kessler et al. (2009b)), and the Panoramic Survey Tele-
 286 scope and Rapid Response System, (Pan-STARRS), su-
 287 pernova survey Kaiser et al. (2010); Jones et al. (2018);
 288 Scolnic et al. (2018) and those observed by the Hubble
 289 Space Telescope (HST) Riess et al. (2007); Jones et al.
 290 (2013).

291 The observations of Type Ia supernova from Pan-
 292 STARRS, (PS1), were accessed from the site <https://archive.stsci.edu/prepds/ps1cosmo/jones> and the file
 293 datatable.html. In 2018 Pan-STARRS consisted of two
 294 1.8-m Ritchey-Chrétien telescopes located at Haleakala
 295 in Hawaii and could record almost 1.4 billion pixels per
 296 image. It is designed to detect moving or variable ob-
 297 jects on a continual basis. An image with a 30 to 60
 298 second duration can record down to an apparent magni-
 299 tude of 22 mag. The whole visible sky will be surveyed
 300 four times a month.

302 Although theoretically, the Type Ia supernova model
 303 has a fixed absolute magnitude, its measurement is sub-
 304 ject to the usual uncertainties. This is why they can be
 305 observed at redshifts beyond the nominal limit of the
 306 telescope and are subject to Malmquist bias.

307 However many of the observations come from the PS1
 308 survey which is essentially providing a continuous record
 309 of the sky so that the simple Malmquist bias is not appli-
 310 cable. However for all the other supernova a Malmquist
 311 bias of $-1.382\sigma_i^2$ mag, where σ_i is the observed flux

Table 1. Light-curve numbers for each band

Band	$\lambda/\mu\text{m}$	N^a	N^b
U	0.365	77	0
B	0.445	121	0
V	0.551	121	0
R	0.658	72	0
I	0.809	74	0
u	0.354	141	0
g	0.475	421	1141
r	0.622	468	1132
i	0.763	468	1142
z	0.905	412	1146
F775W	0.771	7	0
F850LP	0.907	17	0

^a Number of supernova from other catalogues.

^b Number of supernova for the PS1 catalogue.

312 density uncertainty was applied. (The application of
 313 Malmquist bias corrections made negligible difference to
 314 the results.)

315 Table 1 shows the statistics for the selected supernova.
 316 The selection criteria was that there was a good fit and
 317 the width was between 0.3 and 5.0 and the width uncer-
 318 tainly was less than 0.3. In addition the value of \mathcal{L} had
 319 to be less than $20/n$.

320 2.4. Results for the light curve width

321 from 1,745 initial candidates there were 1,707 that
 322 satisfied selection criteria. Most of the rejections were
 323 because there were insufficient observations prior to the
 324 peak epoch.

325 The important result of this width analysis is a re-
 326 gression of $w_{obs}(z)$ as a function of z for all the 1,707
 327 accepted observations which is

$$w_{obs}(z) = (1.060 \pm 0.009 + (1.080 \pm 0.042))z. \quad (4)$$

329 Although the ordinate is statistically different from
 330 one, it is this ordinate that is most sensitive to calibra-
 331 tion and systematic errors such as having minor errors
 332 in the reference light curve. Here this difference is not
 333 important. However the coordinate shows an excellent
 334 agreement with one. Note that this width is indepen-
 335 dent any cosmological model.

336 The widths for all the supernova are shown in Figure 1.
 337 It is clear that the slope is consistent with the expected
 338 dependence of $w(z) = 1+z$. Some of the supernova show
 339 either discrepant widths or discrepant uncertainties and
 340 to avoid any bias, no rejections have been made to the
 341 original data.

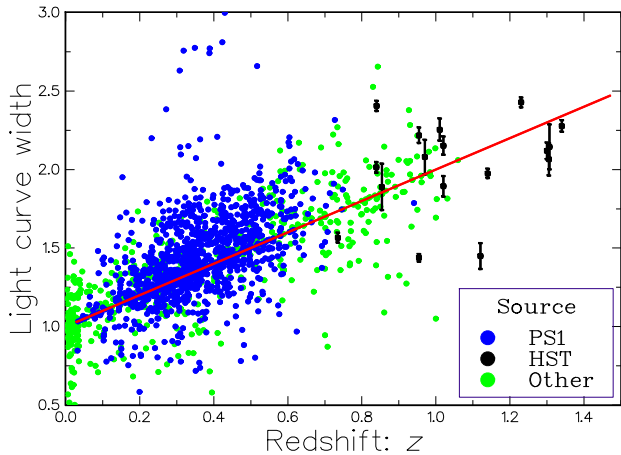


Figure 1. A plot of the Type Ia supernova light curve observed widths. The blue dots are for the PS1 and the black dots with error bars show the HST (Hubble Space Telescope) observations. All other observations are shown by the green dots. The red line shows a $(1+z)$ dependence

For convenience it helps to convert all the flux densities into magnitudes. All computed apparent magnitudes except the those in the SDSS catalogue were calculated by $m_k = 27.5 - 2.5 \log_{10}(F_k)$ where F_k is the peak flux density and k is the band. Those in the SDSS catalogue had $m_k = 24.5 - 2.5 \log_{10}(F_k)$.

Since each supernova has a peak flux density for each observed band, they can be combined to provide a peak intrinsic flux density for each band and a cosmological flux density for the supernova. Thus there is a clear separation between the intrinsic flux density which is independent of the redshift and the cosmological redshift that is only a function of redshift.

Then for each supernova and band the fitted apparent magnitude is the sum of an intrinsic magnitude and a common cosmological magnitude. Starting with a constant intrinsic flux density, the average magnitude was determined by fitting a regression equation to the observed peak magnitudes minus the current intrinsic magnitude which is common to all the supernova and is a function of the intrinsic wavelength.

The first step is to estimate an initial cosmological flux density as the mean of the observed peak flux densities for each band. The next step is to determine an estimate of the intrinsic flux density as a function of the intrinsic wavelength, ψ which by definition is

$$\psi = \lambda / (1 + z). \quad (5)$$

Initially there 30 boxes that cover the ψ range are set to zero, then the difference between each observed flux density and the current estimate of the absolute magnitude is added to the appropriate box. After all the observa-

tions are processed, the procedure is repeated with each peak flux density being corrected for the average flux density defined by the mean of its box. Then a new set of cosmological magnitudes are produced. This process is repeated until the are legible changes in all the values.

Thus each supernova has a peak cosmological magnitude and there is a common intrinsic magnitude distribution. The individual intrinsic peak magnitude data points for the supernova are shown in Figure 2 and tabulated in Table 2. There is a very rapid decrease in the intrinsic luminosity as the intrinsic wavelength approaches the Lyman $_{\alpha}$ line which suggests scattering in a local hydrogen cloud. This could also explain the lack of hydrogen lines in the spectra. Note that the size of this cloud would be very small and would not be easily detected.

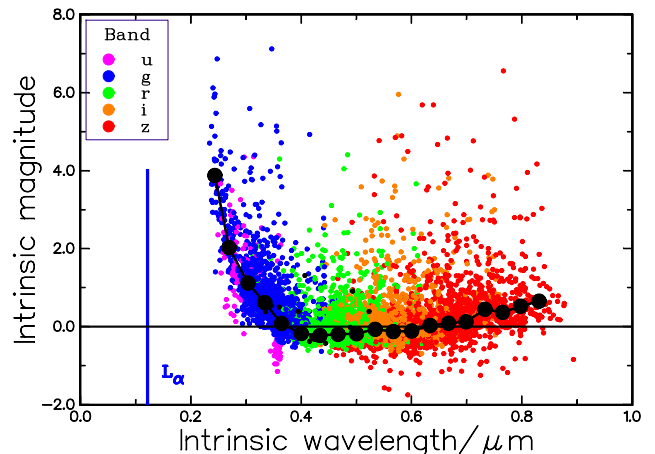


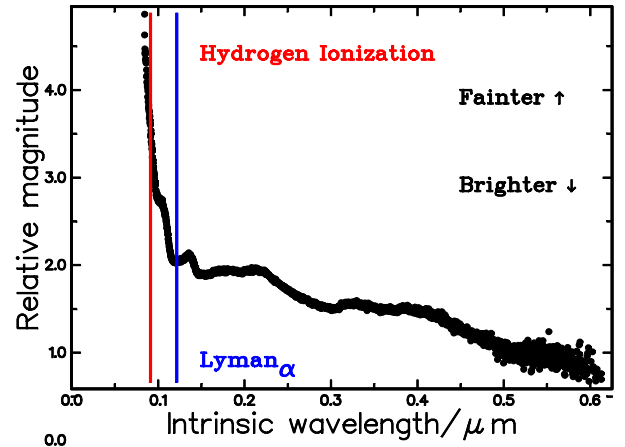
Figure 2. The intrinsic peak magnitude of Type Ia supernova as a function of intrinsic wavelength, ψ . The black points and curve show the average intrinsic peak magnitude as a function of intrinsic wavelength. The bands $UBVRI$ have the same sequential colors as the bands $ugriz$. The position of the Lyman $_{\alpha}$ line is shown in blue.

The purpose of this section is to show that an analysis of the observed magnitudes for many quasars is to show that they all have a relative energy loss of $(1+z)$.

From Wikipedia: “A quasar also known as a quasi-stellar object is an extremely luminous active galactic nucleus (AGN), powered by a supermassive black hole, with mass ranging from millions to tens of billions times the mass of the Sun, surrounded by a gaseous accretion disc. Gas in the disc falling towards the black hole heats up because of friction and releases energy in the form of electromagnetic radiation. The radiant energy of quasars is enormous; the most powerful quasars have luminosities thousands of times greater than a galaxy such as the Milky Way. Usually, quasars are categorized

Table 2. Intrinsic magnitude of Type Ia supernova

box	number	$\psi/\mu\text{m}$	magnitude
8	26	0.243	3.876 ± 0.247
9	132	0.269	2.021 ± 0.077
10	256	0.304	1.113 ± 0.051
11	471	0.334	0.613 ± 0.032
12	608	0.364	0.080 ± 0.027
13	470	0.400	-0.181 ± 0.022
14	521	0.434	-0.227 ± 0.021
15	537	0.467	-0.197 ± 0.021
16	493	0.500	-0.182 ± 0.023
17	499	0.534	-0.067 ± 0.030
18	498	0.567	-0.126 ± 0.033
19	453	0.600	-0.114 ± 0.029
20	383	0.634	0.027 ± 0.039
21	368	0.667	0.086 ± 0.038
22	265	0.699	0.126 ± 0.042
23	190	0.733	0.443 ± 0.059
24	106	0.765	0.366 ± 0.084
25	100	0.798	0.520 ± 0.093

**Figure 3.** The black plot shows the average intrinsic magnitude of SDSS quasars as a function of intrinsic wavelength, ψ . The position of the wavelength for the Lyman α line is shown in blue and that for the hydrogen ionization is shown in red.

as a subclass of the more general category of AGN. The redshifts of quasars are of cosmological origin.”

All quasar data used here is taken from the Sloan Digital Sky Survey Quasar Catalog: Sixteenth Data Release (DR16Q) Lyke et al. (2020).

The majority of these quasars have been discovered by a flux density limited survey without knowledge of the redshift and it is clear that the observed magnitudes have a very limited dependence on their observed redshift. Thus the observation model is that the selection of each quasar is determined by the cut-off flux density and the overall telescope noise and it is assumed that these values are the same for all the quasars.

Thus for each quasar discovered its apparent magnitude must lie in the range of magnitudes that are accepted by the telescope and it is completely independent of the intrinsic magnitude of the quasar. The observed flux density depends on the probability of seeing the quasar and its distance. Since the observed distance is rapidly increasing with redshift, it is proportional to the maximum area. For this distance the observed flux density is inversely proportional to the same area. Since these two areas cancel each other, the expected flux density is the cut-off flux density plus, if any, common cosmological flux density.

The data for each quasar is its redshift and the observed magnitudes for the 5 bands, $UBVRI$. The intrinsic magnitude for each band is determined by the procedure described in section 2.3 for the supernova, except there were 1000 boxes.

The quasar intrinsic magnitude is shown in Figure 3. The rapid decrease in luminosity at short wavelengths is probably due to a local hydrogen cloud. Note that if quasars are like black holes then the size of this cloud could be very small and it would not easily be detected against the luminosity of the accretion disk.

If the universe is expanding then this energy loss factor is proportional to $(1+z)^{-1}$. A simple method to measure this average energy loss is to assume that the expected magnitude is

$$m = a + b \times 2.5 \log_{10}(1+z) \quad (6)$$

Then the expected values are $a = -1$ and $b = -1$. The weighted regression equation for 635,218 quasars produced the results $a = -0.9109 \pm 0.001$ and

$$b = -(1.0073 \pm 0.0046). \quad (7)$$

The difference of the parameter a from -1 is unknown but fortunately it is not important here. However the agreement of parameter b with -1 is very clear and shows very strong support for an energy loss rate of $1/(1+z)$.

2.5. Supernova absolute magnitudes.

The absolute magnitude of Type Ia supernova is the sum of the apparent magnitude and a distance modulus.

Scolnic et al. (2017) suggests several distance moduli that have a good fit to the PS1 Medium Deep Survey that were analyzed with the SALT2 method. The simplest is the Λ CDM model. There are two sets of data, the 1117 PS1 set and the combined 1652 described above that can be used to test the absolute magnitude dependence on redshift. The PS1 set (JonesJones et al. (2018)

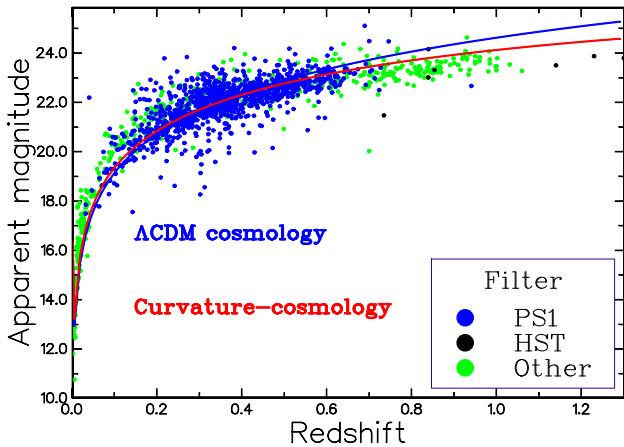


Figure 4. The cosmological apparent magnitude of the current Type Ia supernova as a function of redshift. The blue curve is the distance modulus for the Λ CDM model. The red curve is the distance modulus for Curvature-cosmology.

462 table (3)) is a list of results from the Pan-STARRS
 463 supernova survey and their apparent magnitudes have
 464 been corrected using Scolnic et al. (2017) Eq.(3) and
 465 using the Λ CDM model, the regression of the absolute
 466 magnitude verse redshift for the 1117 PS1 Type Ia su-
 467 pernova that used the SALT2 model

$$M(z) = -19.216 \pm 0.009 + (0.052 \pm 0.067)z, \quad (8)$$

468 where the last term is statistically equal to zero. This
 469 shows that the SALT2 method is consistent with the
 470 Λ CDM model.

471 However the regression for the 1652 PS1 Type Ia
 472 supernova, using the intrinsic analysis and the Λ CDM
 473 model, is

$$M(z) = -19.244 \pm 0.009 + (0.833 \pm 0.072)z, \quad (9)$$

474 where the last term is not equal to zero.

475 2.6. Discussion of SALT2 supernova magnitudes.

476 The absolute magnitudes of PS1 supernova that are
 477 analyzed by the SALT2 method and using the Λ CDM
 478 model show negligible dependence on redshift. However
 479 the absolute magnitudes that are obtained from intrinsic
 480 analysis and using the Λ CDM model shows a statistically
 481 valid dependence on redshift, $\Delta M = (0.833 \pm 0.072)z$
 482 that is inconsistent with the expected value of zero,

483 could this be due to a fault in the intrinsic analy-
 484 sis? Because the intrinsic analysis is completely inde-
 485 pendent of the observed redshift the anomaly must be
 486 present in the observed data and cannot come from the
 487 analysis. Although it is not an independent result, sec-
 488 tion 4.22 shows that there is no Phillip’s relation. The
 489 conclusion is that it must be in SALT2 and there is a

490 corresponding fault in the Λ CDM procedure that coun-
 491 terbalances the fault.. As shown in the appendix the
 492 SALT2 method calibrates a new Type Ia supernova by
 493 comparing its observations against the results for pre-
 494 vious supernova measurements, these results only show
 495 self-consistency and do not provide validation of the flux
 496 densities. However if there is a systematic error in the
 497 previous supernova measurements, it will be transmit-
 498 ted to new observations. Furthermore SALT2 includes
 499 many ad hoc parameters and it is very complex and in-
 500 cludes the nuisance parameter α that is a measure of the
 501 Phillip’s relation between magnitude and redshift.

502 The major support for the Λ CDM model is that it
 503 describes the general relativity model of an unstable ex-
 504 panding universe. This is similar to assuming that a
 505 falling feather should have the same acceleration as a
 506 falling stone, whereas we know that the difference is due
 507 to air resistance. Maybe cosmology needs something like
 508 air resistance such as Curvature-cosmology,

509 Crucially the standard procedure is to use Λ CDM or
 510 one of its variants to determine the dimensionless den-
 511 sity parameters, which depend on assumptions of infla-
 512 tion, dark matter and dark energy. Since none of these
 513 properties are substantiated by other independent ob-
 514 servations, they do not provide any support for this cos-
 515 mology. Moreover they are ad hoc models largely deter-
 516 mined by supernova observations. In other words, there
 517 are no observations other than those for supernova that
 518 show strong confirmation of the SALT2 analysis and the
 519 Λ CDM model.

520 3. PART B: CURVATURE-COSMOLOGY THEORY.

521 3.1. Introduction

522 Curvature-cosmology is a static tired-light cosmology
 523 which is based on the two hypothesizes of Curvature-
 524 redshift which is based on the propagation of a wave
 525 in of curved space-time and Curvature-pressure which
 526 opposes the mutual gravitational attraction of hot gases.

527 It is a static solution to the equation of general relativity
 528 that is described by the Friedmann equations with an
 529 additional term that stabilizes the solution. This term
 530 called Curvature-pressure is a reaction of high-speed
 531 particles back on the material producing the curved
 532 space-time. This sense of this reaction is to try and
 533 reduce the curvature.

534 The basic cosmological model is one in which the cos-
 535 mic plasma dominates the mass distribution and hence
 536 the curvature of space-time. In this first-order model,
 537 the gravitational effects of stars and galaxies are ne-
 538 glected. The geometry C is that of a three-dimensional
 539 “surface’ of a four-dimensional hyper-sphere, which is
 540 common to most cosmologies.

541 For a static universe, there is no ambiguity in the
 542 definition of distances and times. One can use a uni-
 543 versal cosmic time and define distances in light travel
 544 times or any other convenient measure. In a statistical
 545 sense Curvature-cosmology obeys the perfect cosmolog-
 546 ical principle of being the same at all places and at all
 547 times.

548 Curvature-cosmology makes quite specific predictions
 549 that can be refuted. Thus, any observations that unam-
 550 biguously show changes in the universe with a redshift
 551 would invalidate it. In Curvature-cosmology, there is a
 552 continuous process in which some of the cosmic gas will
 553 aggregate to form galaxies and then stars. The galaxies
 554 and stars will evolve and eventually all their material
 555 will be returned to the cosmic plasma. Thus, a char-
 556 acteristic of Curvature-cosmology is that although in-
 557 dividual galaxies will be born, live and die, the overall
 558 population will be statistically the same for any observ-
 559 able characteristic.

560 3.2. Derivation of Curvature-redshift

561 The derivation of Curvature-redshift is based on the
 562 fundamental hypothesis of Einstein's general theory of
 563 relativity that space is curved. As a consequence, the
 564 trajectories of initially parallel point particles, geodesics,
 565 will move closer to each other, or further apart as time
 566 increases. Consequently in space with a positive cur-
 567 vature, the cross-sectional area of a bundle of geodesics
 568 will slowly decrease.

569 In applying this idea to photons, we assume that a
 570 photon is described in quantum mechanics as a local-
 571 ized wave where the geodesics correspond to the rays of
 572 the wave. Note that this wave is quite separate from
 573 an electromagnetic wave that corresponds to the effects
 574 of many photons. It is fundamental to the hypothesis
 575 that we can consider the motion in space of individual
 576 photons.

577 Because the curvature of space causes the focusing of a
 578 bundle of geodesics, this focusing also applies to a wave.
 579 As the photon progresses, the cross-sectional area of the
 580 wave associated with it will decrease. However, in quan-
 581 tum mechanics properties such as angular momentum
 582 are computed by an integration of a radial coordinate
 583 over the volume of the wave and will be affected by the
 584 focusing.

585 If the cross-sectional area of the wave decreases, then
 586 the angular momentum will also decrease. However, an-
 587 gular momentum is a quantized parameter that for pho-
 588 tons has a fixed value. The solution to this dilemma
 589 is that, from symmetry, the photon splits into two very
 590 low-energy photons and a third that has the same direc-
 591 tion as the original photon and nearly all the energy.

592 Since in quantum mechanics protons and other parti-
 593 cles are considered as waves, a similar process will also
 594 apply. It is argued that protons and other particles will
 595 interact with curved space to lose energy by the emission
 596 of very low-energy photons.

597 Einstein's general theory of relativity requires that the
 598 metric of space-time be determined by the distribution
 599 of mass (and energy). In general this space-time will be
 600 curved such that in a space of positive curvature, nearby
 601 geodesics that are initially parallel will come closer to-
 602 gether as the reference position moves along them. This
 603 is directly analogous to the fact that on the earth lines
 604 of longitude come closer together as they go from the
 605 equator to either pole. In flat space-time, the separa-
 606 tion remains constant.

607 The *equation for geodesic deviation* can be written
 608 Misner, Thorne, & Wheeler (1973) as

$$\frac{d^2\xi}{dr^2} = -\frac{\xi}{R^2},$$

609 where ξ is a distance normal to the trajectory and r is
 610 measured along the trajectory. The quantity $1/R^2$ is the
 611 Gaussian curvature at the point of consideration.

612 The experiment of using single photons in a two-slit
 613 interferometer shows that individual photons must have
 614 a finite size. Quantum mechanics requires that all par-
 615 ticles are described by wave functions and therefore we
 616 must consider the propagation of a wave in space-time.
 617 Because photons are bosons, the usual quantum me-
 618 chanical approach is to describe the properties of pho-
 619 tons by creation and destruction operators.

620 However, in any other reference frames they behave
 621 like normal particles with definite trajectories and life-
 622 times. Although Havas (1966) has pointed out that the
 623 concept of a single photon is rather tenuous. There is no
 624 way we can tell the difference between a single photon
 625 and a bundle of photons with the same energy, momen-
 626 tum, and spin. Nevertheless, it is an essential part of
 627 this derivation that a single photon has an actual exist-
 628 ence.

629 Assume that a photon can be described by a local-
 630 ized wave packet that has finite extent both along and
 631 normal to its trajectory. This economic description is
 632 sufficient for the following derivation. From de Broglie's
 633 equation the frequency of a photon with energy E is
 634 $\nu = E/h$ and its wavelength as $\lambda = hc/E$ where E is its
 635 energy. These definitions are for convenience and do not
 636 imply that we can ascribe a frequency or a wavelength
 637 to an individual photon; they are properties of groups of
 638 photons. The derivation requires that the wavelength is
 639 short compared to the size of the wave packet and that
 640 this is short compared to variations in the curvature of
 641 space-time.

642 Furthermore, we assume that the rays follow null
 643 geodesics and therefore any deviations from flat space-
 644 time produce change in shape of the wave packet. In
 645 other words, since the scale length of deviations from flat
 646 space are large compared to the size of the wave packet
 647 they act as a very small perturbation to the propagation
 648 of the wave packet.

649 Consider a wave packet moving through a space-time
 650 of constant positive curvature. Because of geodesic de-
 651 viation, the rays come closer together as the wave packet
 652 moves forward. They are focused. In particular the di-
 653 rection θ , of a ray (geodesic) with initial separation ξ
 654 after a distance r is (assuming small angles)

$$\theta = -\frac{r\xi}{R^2},$$

655 where R is the radius of curvature.

656 Since the central geodesic is the direction of energy
 657 flow, we can integrate the wave-energy-function times
 658 the component of θ normal to the trajectory, over the
 659 dimensions of the wave packet in order to calculate the
 660 amount of energy that is now traveling normal to the
 661 trajectory. The result is a finite energy that depends
 662 on the average lateral extension of the wave packet, the
 663 local radius of curvature, and the original photon energy.

664 The actual value is not important but rather the fact
 665 that there is a finite fraction of the energy that is mov-
 666 ing away from the trajectory of the original wave packet.
 667 This suggests a photon interaction in which the pho-
 668 ton interacts with curved space-time with the hypoth-
 669 esis that the energy flow normal to the trajectory goes
 670 into the emission of secondary photons normal to its
 671 trajectory.

672 From a quantum-mechanical point of view, there is a
 673 strong argument that some interaction must take place.
 674 If the spin of the photon is directly related to the angular
 675 momentum of the wave packet about its trajectory then
 676 the computation of the angular momentum is a similar
 677 integral.

678 Then because of *focussing* the angular momentum
 679 clearly changes along the trajectory, which disagrees
 680 with the quantum requirement that the angular momen-
 681 tum, that is the spin, of the photon is constant. The
 682 Heisenberg uncertainty principle requires that an incor-
 683 rect value of spin can only be tolerated for a small time
 684 before something happens to restore the correct value.
 685 We now consider the consequences.

686 Consider motion on the surface of a three-dimensional
 687 sphere with radius r . As described above, two adjacent
 688 geodesics will move closer together due to focusing. Sim-
 689 ple kinematics tells us that a body with velocity v asso-
 690 ciated with these geodesics has acceleration v^2/r , where

691 r is the radius of curvature. This acceleration is directly
 692 experienced by the body.

693 The geometry of a three-dimensional ‘surface’ with
 694 curvature in the fourth dimension is essentially the same
 695 as motion in three dimensions except that the focusing
 696 now applies to the cross-sectional area and not to the
 697 separation.

698 Since wave packet that is subject to focusing has ac-
 699 celeration in an orthogonal dimension will also experi-
 700 ence an acceleration of c^2/r normal to the surface of the
 701 sphere. Then a wave packet (and hence a photon) that
 702 has its cross-sectional area focused by curvature in the
 703 fourth dimension with radius r would have an energy
 704 loss rate proportional to this acceleration. The essence
 705 of the Curvature-redshift hypothesis is that the focus-
 706 ing causes the photon to interact and that the energy
 707 loss rate is proportional to c^2/R . For a photon with en-
 708 ergy E the loss rate per unit time is cE/R , and per unit
 709 distance it is E/R .

710 In general relativity the crucial equation for the focus-
 711 ing of a bundle of geodesics was derived by Raychaud-
 712 huri (1955), also see Misner et al. (1973) and Ellis (1984)
 713 and for the current context we can assume that the bun-
 714 dle has zero shear and zero vorticity. Since any change
 715 in geodesic deviation along the trajectory will not alter
 716 the direction of the geodesics, we need consider only the
 717 cross-sectional area A of the geodesic bundle to get the
 718 equation

$$\frac{1}{A} \frac{d^2 A}{dr^2} = -\mathbf{R}_{\alpha\beta} \mathbf{U}^\alpha \mathbf{U}^\beta = -\frac{1}{R^2}, \quad (10)$$

719 where \mathbf{R} is the Ricci tensor (it is the contraction of the
 720 Riemann-Christoffel tensor), \mathbf{U} is the 4-velocity of the
 721 reference geodesic and R is the local radius of curva-
 722 ture. This focusing can be interpreted as the second
 723 order rate of change of cross-sectional area of a geodesic
 724 bundle that is on the three-dimensional surface in four-
 725 dimensional space. Then if we consider that a photon is
 726 a wave packet we find that the rate at which the photon
 727 loses energy per unit distance is E/R or more explicitly

$$\frac{1}{E} \frac{dE}{dr} = -\frac{1}{R} = -(\mathbf{R}_{\alpha\beta} \mathbf{U}^\alpha \mathbf{U}^\beta)^{1/2}, \quad (11)$$

728 What is interesting about this equation is that, for the
 729 Schwarzschild (and Kerr) solutions for the external field
 730 for a mass, the Ricci tensor is zero; hence, there is no
 731 focusing and no energy loss. A geodesic bundle passing
 732 a mass such as the sun experiences a distortion but the
 733 wave packet has not changed in area. Hence, this model
 734 predicts that photons passing near the limb of the sun
 735 will not suffer any energy loss due to curvature redshift.

3.3. Gravitation is not a force

737 The phrase *gravitational force* is not only a popular
 738 expression but is endemic throughout physics. In par-
 739 ticular, gravitation is classified as one of the four funda-
 740 mental forces with its heritage going back to Newton’s
 741 law of gravitation. I argue that the formulation of grav-
 742 itation as a force is a misconception. In both Newtonian
 743 theory and general relativity, gravitation is acceleration.
 744 To begin let us examine the original Newtonian gravita-
 745 tion equation

$$m_i \mathbf{a} = \mathbf{F} = -\frac{GMm_G}{r^3} \mathbf{r}, \quad (12)$$

746 where (following Longair (1991)) we identify m_i as the
 747 inertial mass of the test object, M as the active gravita-
 748 tional mass of the second object and m_G as the passive
 749 gravitational mass of the test object. The vector \mathbf{a} is its
 750 acceleration and \mathbf{r} is its displacement from the second
 751 object. This equation is usually derived in two steps:
 752 first, the derivation of a gravitational field and second,
 753 the force produced by that field on the test mass. By
 754 analogy with Coulomb’s law, the passive gravitational
 755 mass has a similar role to the electric charge.

756 However many experiments by Eötvös, Pekár, &
 757 Fekete (1922), Dicke (1964), and Braginskij & Panov
 758 (1971) have shown that the passive gravitational mass
 759 is equal to the inertial mass to about one part in 10^{12} .
 760 The usual interpretation of the agreement is that they
 761 are fundamentally the same thing. However, an alterna-
 762 tive viewpoint is that the basic equation is wrong and
 763 that the passive gravitational mass and the inertial mass
 764 should not appear in the equation. In this case the cor-
 765 rect equation is

$$\mathbf{a} = -\frac{GM}{r^3} \mathbf{r}. \quad (13)$$

766 Thus, the effect of gravitation is to produce accelera-
 767 tions directly; there is no force involved. Some might
 768 argue that since the two masses cancel the distinction is
 769 unimportant. On the other hand, I would argue that the
 770 application of Ockham’s razor dictates the use of Eq. 13
 771 instead of Eq. 12.

772 The agreement of the inertial mass with the passive
 773 gravitational mass is the basis of the weak equivalence
 774 principle in that it applies regardless of the composition
 775 of the matter used. Carlip (1998) Shows that it applies
 776 to both the potential and the kinetic energy in the body.
 777 The theory of general relativity is based on the principle
 778 of equivalence as stated by Einstein: *All local, freely*
 779 *falling, non-rotating laboratories are fully equivalent for*
 780 *the performance of physical experiments.*

781 The relevance here is that it is impossible to distin-
 782 guish between acceleration and a uniform gravitational
 783 field. Thus when gravitation is considered as accelera-

784 tion and not a force the passive gravitational mass is a
 785 spurious quantity that is not required by either theory.

3.4. Derivation of Curvature-pressure.

787 The hypothesis of Curvature-pressure is that for mov-
 788 ing particles there is a pressure generated that acts back
 789 on the matter that causes the curved space-time. In this
 790 case, Curvature-pressure acts on the matter (plasma)
 791 that is producing curved space-time in such a way as
 792 to try to decrease the curvature. In other words, the
 793 plasma produces curved space-time through its den-
 794 sity entering the stress-energy tensor in Einstein’s field
 795 equations and the constraint of the plasma to a three-
 796 dimensional hyper-“surface”.

797 A simple cosmological model using Newtonian physics
 798 in four-dimensional space illustrates some of the ba-
 799 sic physics subsequently used to derive the features
 800 of Curvature-pressure. The model assumes that the
 801 universe is composed of plasma confined to the three-
 802 dimensional “surface” of a four-dimensional hypersphere.

803 Since the visualization of four dimensions is difficult
 804 let us suppress one of the normal dimensions and con-
 805 sider the gas to occupy the two-dimensional surface of a
 806 normal sphere. From Gauss’s law (i.e. the gravitational
 807 effect of a spherical distribution of particles with radial
 808 symmetry is identical to that of a point mass equal in
 809 value to the total mass situated at the center of symme-
 810 try) the gravitational acceleration at the radius r of the
 811 surface is normal to the surface, directed inward and it
 812 has the magnitude

$$\ddot{r} = -\frac{GM}{r^2}, \quad (14)$$

813 where M is the total mass of the particles and the dots
 814 denote a time derivative. For equilibrium, and assuming
 815 all the particles have the same mass and velocity we
 816 can equate the radial acceleration to the gravitational
 817 acceleration and get the simple equation from celestial
 818 mechanics of

$$\frac{v^2}{r} = \frac{GM}{r^2}.$$

819 If there is conservation of energy, this stable situation is
 820 directly analogous to the motion of a planet about the
 821 sun.

822 When there is a mixture of particles with different
 823 masses, there is an apparent problem. In general, parti-
 824 cles will have a distribution of velocities and the heavier
 825 ones can be expected to have, on average, lower veloci-
 826 ties. Thus, equilibrium radii will vary with the velocity
 827 of the particles.

828 However, the basis of this model is that all particles
 829 are constrained to have the same radius regardless of
 830 their mass or velocity with the value of the radius set

831 by the average radial acceleration. Thus for identical
832 particles with a distribution of velocities we average over
833 the squared velocities to get

$$\langle v^2 \rangle = \frac{GM}{r}. \quad (15)$$

834 If there is more than one type of particle with different
835 masses then we invoke the precepts of Section 3.3 and
836 average over the accelerations to get the same result.
837 The effect of this balancing of the accelerations against
838 the gravitational potential is seen within the shell as a
839 Curvature-pressure that is a direct consequence of the
840 geometric constraint of confining the particles to a shell.

841 If the radius r decreases then there is an increase in
842 this Curvature-pressure that attempts to increase the
843 surface area by increasing the radius. For a small change
844 in radius in a quasi-equilibrium process where the par-
845 ticle velocities do not change the work done by this
846 Curvature-pressure (two dimensions) with an incremen-
847 tal increase of area dA is $p_c dA$ and this must equal the
848 gravitational force times the change in distance to give

$$p_c dA = \frac{GM^2}{r^2} dr,$$

849 where $M = \sum m_i$ with the sum going over all the par-
850 ticles and the negative sign shows that it is opposite
851 in effect to thermodynamic pressure. Therefore, using
852 Eq. 15 we can rewrite the previous equation in terms of
853 the velocities as

$$p_c dA = \frac{M \langle v^2 \rangle}{r} dr.$$

854 Now $dA/dr = 2A/r$, hence the two-dimensional
855 Curvature-pressure is

$$p_c = \frac{M \langle v^2 \rangle}{2A}.$$

856 This simple Newtonian model provides a guide as to
857 what the Curvature-pressure would be in the full general
858 relativistic model.

859 In deriving a more general model in analogy to the
860 Newtonian one, we first change $dA/dr = 2A/r$ to
861 $dV/dr = 3V/r$ (where V is the volume) and secondly
862 we include the correction γ^2 needed for relativistic ve-
863 locities which refers to the dominant massive particles.
864 The result is

$$p_c = \frac{\langle \beta^2 \rangle Mc^2}{3V} = \frac{\langle \gamma^2 - 1 \rangle Mc^2}{3V}. \quad (16)$$

865 Note that the 3 is the number of degrees of freedom.
866 In this case the constraint arises from the confinement
867 of all the particles within a three-dimensional hyper-
868 ‘surface’. Now we expect to be dealing with fully ionized

869 high temperature plasma with a mixture of electrons,
870 protons, and heavier ions where the averaging is done
871 over the accelerations. Define the average density by
872 $\rho = M/V$ then the cosmological Curvature-pressure is

$$p_c = \frac{1}{3} \langle 1 - \gamma^2 \rangle \rho c^2. \quad (17)$$

873 In effect, my hypothesis is that the cosmological model
874 must include this Curvature-pressure as well as ther-
875 modynamic pressure. Note that although this has a
876 similar form to thermodynamic pressure it is quite dif-
877 ferent. In particular, it is proportional to an average
878 over the squared velocities and the thermodynamic pres-
879 sure is proportional to an average over the kinetic en-
880 ergies. This means that, for plasma with free electrons
881 and approximate thermodynamic equilibrium, the elec-
882 trons will dominate the average due to their much larger
883 velocities. From a Newtonian point of view, Curvature-
884 pressure is opposed to gravitational mutual acceleration.

885 In general relativity, the plasma produces curved
886 space-time through its density entering the stress-energy
887 tensor in Einstein’s field equations. Then the constraint
888 of confining the particles to a three-dimensional shell
889 produces a pressure whose reaction is the Curvature-
890 pressure acting to decrease the magnitude of the curva-
891 ture and hence decrease the density of the plasma.

892 3.5. The Curvature-cosmological model

893 Curvature-cosmology can now be derived by includ-
894 ing Curvature-redshift and Curvature-pressure into the
895 equations of general relativity. This is done by using ho-
896 mogeneous isotropic plasma as a model for the real uni-
897 verse. The general theory of relativity enters through
898 the Friedmann equations for a homogeneous isotropic
899 gas.

900 Although such a model is simple compared to the real
901 universe, the important characteristics of Curvature-
902 cosmology can be derived by using this model. The
903 first step is to obtain the basic relationship between the
904 density of the gas and the radius of the universe. The
905 inclusion of Curvature-pressure is not only important
906 in determining the basic equations but it also provides
907 the necessary means of making the solution static and
908 stable.

909 Then it is shown that the effect of Curvature-redshift
910 is to produce a redshift that is a function of distance,
911 and the slope of this relationship is (in the limit of small
912 distances) the Hubble constant.

913 The first-order model considers the universe to be a
914 gas with uniform density and complications such as den-
915 sity fluctuations, galaxies, and stars are ignored. In ad-
916 dition, we assume (to be verified later) that the gas is

at high temperature and is fully ionized plasma. Because of the high symmetry, the appropriate metric is the one that satisfies the equations of general relativity for a homogeneous, isotropic gas.

Based on the Robertson-Walker metric, the Friedmann equations for the homogeneous isotropic model with constant density and pressure without the cosmological constant and with $k = 1$ are (Longair 1991)

$$\begin{aligned}\dot{R}^2 &= \frac{8\pi G\rho}{3} R^2 - c^2 \\ \ddot{R} &= -\frac{4\pi G}{3} \left(\rho + \frac{3p}{c^2} \right) R,\end{aligned}\quad (18)$$

where R is the radius, ρ is the density, p is the thermodynamic pressure, G is the Newtonian gravitational constant and the superscript dots denote time derivatives.

Assuming that the thermodynamic pressure is negligible and including the Curvature-pressure, Eq. 17, the second modified Friedmann equation is

$$\ddot{R} = -\frac{4\pi G\rho}{3} [1 + \langle 1 - \gamma^2 \rangle] R, \quad (19)$$

Clearly, there is a static solution with $\ddot{R} = 0$ which means that $\gamma^2 = 2$.

The first Friedmann equation provides the radius of the universe which is

$$\begin{aligned}R &= \sqrt{\frac{3c^2}{8\pi G\rho}} \text{ m} \\ &= 1.268 \times 10^{13} / \sqrt{\rho} \text{ m} \\ &= 3.112 \times 10^{26} / \sqrt{N_\epsilon} \text{ m} \\ &= 1.008 \times 10^4 / \sqrt{N_\epsilon} \text{ Mpc}\end{aligned}\quad (20)$$

where N_ϵ is the number density measured in number of hydrogen atoms per m^3 .

The basic instability of the static Einstein model is well known (Tolman 1934; Ellis 1984). On the other hand, the effect of Curvature-pressure is opposite in effect to the normal pressure thus Curvature-cosmology is intrinsically stable.

Now the apparent ‘‘velocity’, $v(z)$ is the rate of change of z and by definition $dr/dt = c$, thus

$$v(z) = \frac{dz}{dt} = c \frac{dz}{dr} = \frac{c(1+z)}{R}. \quad (21)$$

Since Hubble’s equation is equal to this velocity it is

$$H(z) = \frac{c(1+z)}{R}, \quad (22)$$

and Hubble’s constant is $H_0 = c/r$ and has the value

$$\begin{aligned}H_0 &= c/R \text{ s}^{-1} \\ &= 2.364 \times 10^{-5} \sqrt{\rho} \text{ s}^{-1} \\ &= 9.6352 \times 10^{-19} \sqrt{N_\epsilon} \text{ s}^{-1} \\ &= 29.73 \sqrt{N_\epsilon} \text{ kms}^{-1} \text{ Mpc}^{-1} \\ &= 41.30 \text{ kms}^{-1} \text{ Mpc}^{-1},\end{aligned}\quad (23)$$

where the last line has used $N_\epsilon = 1.93$ from section 4.2.

Since $E = ch/\lambda$ and with the redshift and using Eq. 11 provides an important equation which shows the relationship between the cosmic distance and redshift and is

$$\log(E(r)/E_0) = -r/R. \quad (25)$$

Since $z = (\lambda/\lambda_0 - 1)$ then

$$r = R \log(1+z). \quad (26)$$

Integration provides an alternative form for the energy loss which is

$$z = \exp(-r/R) - 1. \quad (27)$$

Of interest is that the distance to the furthest point is $r/R = \pi$ which has a redshift of $z = 22.141$. The light travel time to that point is $\pi R/c = 7.439 \times 10^{10}$ years.

3.6. Distance modulus.

The geometry of Curvature-cosmology is that of a three-dimensional ‘‘surface’ of a four-dimensional hypersphere with radius R . For this geometry the area is

$$A(r) = 4\pi[R \sin(r/R)]^2.$$

Let a source have a luminosity $L(\nu)$ (W Hz^{-1}) at the emission frequency ν . Then if energy is conserved, the observed flux density, $F(\nu)$ ($\text{W m}^{-2} \text{ Hz}^{-1}$) at a distance parameter z is the luminosity divided by the area, which is

$$F(\nu) d\nu = \frac{L(\nu) d\nu}{4\pi[R \sin(r/R)]^2}.$$

However, because of Curvature-redshift there is an energy loss such that the received frequency ν_0 is related to the emitted frequency ν_e by $(\nu_0 = (1+z)\nu_e)$. Including this the result and Eq. 25 it is

$$F(\nu_0) d\nu_0 = \frac{L(\nu_0) d\nu_0}{4\pi[R \sin(\log(1+z))]^2 (1+z)}.$$

since the absolute magnitude is the apparent magnitude when the object is at a distance of 10 pc then

$$F_{10}(\nu_0) d\nu_0 = \frac{1}{10 \text{ pc}/R},$$

974 where because 10 pc is negligible compared to R , ap- 1007
 975 proximations have been made. The flux density ratio 1008
 976 is

$$F(\nu_0) = \left[\frac{10pc/R}{\sin(\log(1+z))} \right]^2 \left\{ \frac{1}{1+z} \right\}.$$

977 The apparent magnitude is defined as $m = -2.5 \log(S)$ 1012
 978 where the base of the logarithm is 10 and the constant 1013
 979 2.5 is exact and M as the absolute magnitude we get 1014
 980 the distance modulus, $\mu = m - M$ to be

$$\mu = 5 \log_{10}[R \sin(\log(1+z))] + 2.5 \log_{10}(1+z) + 44.304. \quad (28)$$

981 3.7. Temperature of the cosmic plasma

982 One of the most remarkable results of Curvature cos- 1021
 983 mology is that it predicts the temperature of the cosmic 1022
 984 plasma from fundamental constants. That is the pre- 1023
 985 dicted temperature is only dependent on the electron 1024
 986 density of the intra-galactic medium.

987 For a stable solution to Eq. 19 we need that $\langle \gamma^2 \rangle =$ 1025
 988 2, where the average (denoted by $\langle \rangle$) is taken over 1026
 989 the proton number densities. Since the total energy for 1027
 990 a particle is γmc^2 the kinetic energy is $E(\gamma - 1)mc^2$. In
 991 this case for protons $E = 3.391E^{-14}$ J and from $E = kT$
 992 the plasma temperature is

$$T = 2.456E9. \quad (29)$$

993 Since electrons and nucleons have wave properties 1028
 994 there are subject to Curvature-redshift where the basi- 1029
 995 c energy loss is $\Delta E = E_0 r/R$, where E_0 is the particle 1030
 996 energy and r is the distance traveled. With a velocity 1031
 997 of βc the distance traveled is $r = \beta ct$ and the rate of 1032
 998 energy loss is

$$\frac{\Delta E}{dt} = \frac{E_0 \beta c}{R} \quad (30)$$

999 The distribution of relativistic particles in equilib- 1033
 1000 rium is the Maxwell-Jöoner distribution. With $\gamma =$ 1034
 1001 $1/\sqrt{1-v^2/c^2}$ it is

$$f(\gamma) = \frac{\gamma^2 \beta}{\theta K_2(1/\theta)} \exp(-\gamma/\theta), \quad (31)$$

1002 where $\theta = kT/mc^2$ and K_2 is the modified Bessel func- 1043
 1003 tion of the second kind.

1004 Here its application requires that θ is a constant value 1044
 1005 then the integral over the range of γ is

$$\frac{\Delta E}{dt} = \frac{\gamma^2 \beta^2 c(\gamma - 1)m_p c^2}{R} \exp(-\gamma/\gamma_0)/A, \quad (32)$$

1006 Where A is the normalization constant and is

$$A = \int_1^\infty \gamma^2 \beta(\exp(-\gamma/\gamma_0)) d\gamma, \quad (33)$$

and where $\gamma_0 = \sqrt{2}$.

1007 As explained earlier this lost energy consists of a pair 1008
 1009 of identical photons whose usual interaction with the 1009
 1010 electrons and photons bring them into thermal equilib- 1010
 1011 rium. Since the total energy must be conserved, the 1011
 1012 energy lost by Curvature-redshift must be radiated by 1012
 1013 the emittance of these photons. Then allowing for the 1013
 1014 nucleon number density $N_e = 1.93$, section 4.2, their 1014
 1015 equilibrium temperature is 2.736K. It will be argued in 1015
 1016 section 4.3 that this radiation is the cosmic microwave 1016
 1017 background radiation.

1018 Clearly, the same analysis can be applied to the free 1018
 1019 electrons. In this case the radiation has a temperature 1019
 1020 of 0.419K with a wavelength of 34.4mm.

1021 3.8. Black holes and Jets

1022 Consider a very small homogeneous mass with a radi- 1022
 1023 us R . Its dynamics are described by the Friedmann 1023
 1024 equations, Eq. 18, and if the acceleration is zero then 1024
 1025 $\dot{R} = 0$ and

$$\frac{8\pi G \rho_0 R_0^2}{3} = c^2,$$

1026 where $\rho_0 = 3m/(4\pi R_0^3)$ is the density. Then the mini- 1027
 1027 mum radius is

$$R_0 = \frac{2Gm}{c^2}. \quad (34)$$

1028 For a simple theoretical black hole, this is the 1028
 1029 Schwarzschild radius.

1030 Since the acceleration is zero, there is an absolute min- 1030
 1031 imum radius and smaller radii are inaccessible. This ob- 1031
 1032 ject has all the external properties of a black hole, such 1032
 1033 as accretion disks. Thus it looks like the theoretical 1033
 1034 black hole but is not a black hole.

1035 If the compact object is rotating there is the tantaliz- 1035
 1036 ing idea that Curvature-pressure may produce the emis- 1036
 1037 sion of material in two jets along the spin axis. Since the 1037
 1038 object will be radiating energy all the time, after climb- 1038
 1039 ing out of the gravitational pit it will have a similar 1039
 1040 temperature to the object before it started to collapse. 1040
 1041 The limiting distance will be determined by the polar 1041
 1042 radius. Thus radii greater than this, such as the equa- 1042
 1043 torial radii will still be able to emit energy that can be 1043
 1044 seen. Thus the object will appear like a doughnut with 1044
 1045 zero radiation at the center and with a very broad jet 1045
 1046 parallel to the spin axis.

1047 This could be the 'jet engine' that produces the astro- 1047
 1048 physical jets seen in stellar-like objects and in many huge 1048
 1049 radio sources. Currently there are no accepted models 1049
 1050 for the origin of these jets.

1051 3.9. Inhibition of Curvature-redshift

from the discussion above it is clear that the process of Curvature-redshift requires a gradual focusing to a critical limit, followed by the emission of secondary photons. It is as if the photon gets slowly excited by the focusing until the probability of secondary emission becomes large enough for it to occur.

If there is any other interaction the excitation due to focusing will be nullified. That is, roughly speaking, Curvature-redshift interaction requires an undisturbed path length of at least $\lambda_{secondary}$ for the interaction to occur. Thus suitable criterion for inhibition to occur is that the competing interaction has an interaction length less than $\lambda_{secondary}$.

Although Compton or Thompson scattering are possible inhibitors, there is another interaction that has a much larger cross-section. This is the coherent multiple scattering that produces refractive index.

In classical electromagnetic theory, the refractive index of a medium is the ratio of the velocity of light in vacuum to the group velocity in the medium. However, in quantum mechanics photons always travel at the velocity of light in vacuum. In a medium, a group of photons appears to have a slower velocity because the individual photons interact with the electrons in the medium and each interaction produces a time delay.

Because the interaction of a photon is with many electrons spread over a finite volume, the only possible result of each interaction is the emission of another photon with the same energy and momentum. Now consider the absorption of a wave. In order to cancel the incoming wave a new wave with the same frequency and amplitude but with opposite phase must be produced. Thus, the outgoing wave will be delayed by half a period with respect to the incoming wave. If the phase difference was not exactly half a period for an electromagnetic wave incident on many electrons, the principle of conservation of energy would be violated.

This simple observation enables us to compute the interaction length for refractive index n . If L is this interaction length then it is

$$L = \frac{\lambda_0}{2|n-1|},$$

where n is the refractive index and the modulus allows for plasma and other materials where the refractive index is less than zero.

Note that L is closely related to the extinction length derived by Ewald and Oseen (see (Jackson 1975) or Born & Wolf (1999)) which is a measure of the distance needed for an incident electromagnetic wave with velocity c to be replaced by a new wave.

For plasmas the refractive index is

$$n \cong 1 - \frac{N_e \lambda_0^2}{2\pi r_0},$$

where N_e is the electron density and r_0 is the classical electron radius. We can combine these two equations to get (for a plasma)

$$L = (N_e r_0 \lambda_0)^{-1}. \quad (35)$$

Thus, we would expect the energy loss to be inhibited if the average Curvature-redshift interaction distance is greater than that for refractive-index interactions. Therefore, we can compute the ratio (assuming a plasma with $N \cong N_e$) to get

$$\lambda_{secondary}/L = 0.0106 N_e^{3/4} \lambda_0^{3/2} \quad (36)$$

This result shows that Curvature-redshift will be inhibited if this ratio is greater than one, which is equivalent to $\lambda_0 \geq 20.7 N_e^{-1/2}$ m. For example, Curvature-redshift for the 21 cm hydrogen line will be inhibited if the electron density is greater than about 10^4 m^{-3} .

3.10. Possible laboratory tests.

It is apparent from the above analysis that to observe the redshift in the laboratory we need to have sufficient density of gas (or plasma) to achieve a measurable effect but not enough for there to be inhibition by the refractive index.

The obvious experiment is to use the Mössbauer effect for γ -rays that enable very precise measurement of their frequency. Simply put, the rays are emitted by nuclei in solids where there is minimal recoil or thermal broadening of the emitted ray.

Since the recoil momentum of the nucleus is large compared to the atomic thermal energies and since the nucleus is locked into the solid so that the recoil momentum is precisely defined, then the γ -ray energy is also precisely defined. The absorption process is similar and has a very narrow line width.

Such an experiment has already been done by Pound & Snider (1965). They measured gravitational effects on 14.4 keV γ -rays from ^{57}Fe being sent up and down a vertical path of 22.5m in helium near room pressure. They found agreement to about 1% with the predicted fractional redshift of 1.5×10^{-15} , whereas fractional Curvature-redshift predicted by Eq. 11 for this density is 1.25×10^{-12} . Clearly, this is much larger.

At γ -ray frequencies, the electrons in the helium gas are effectively free and we can use Eq. 35 to compute the refractive index interaction length. For helium at STP, it is $L = 0.077$ m, which is much less than Curvature-redshift interaction length which for these conditions is

1144 $X=11$ m. Hence, we do not expect to see any significant
1145 Curvature-redshift in their results.

1146 Pound and Snyder did observe one-way frequency
1147 shifts but they were much smaller than Curvature-
1148 redshift and could be explained by other aspects of the
1149 experiment. However, the Pound and Snyder experi-
1150 ment provide a guide to a possible test for the existence
1151 of Curvature-redshift. Because Curvature-redshift has
1152 a different density variation to that for the inhibiting
1153 refractive index it is possible to find a density for which
1154 Curvature-redshift is not inhibited.

1155 Although there is a slight advantage in using heavier
1156 gases than helium due to their higher atomic number to
1157 atomic weight ratio, their increased absorption to γ -rays
1158 rules them out. Hence, we stay with helium and from
1159 Eq. 35 we can compute Curvature-redshift interaction
1160 length to be

$$X = 10.8 \left(\frac{p_0}{p} \right)^{1/4} \text{ m,}$$

1161 where p is the pressure and p_0 is the pressure at STP.
1162 For the same gas the refractive-index interaction length
1163 is

$$L = 0.077 \left(\frac{p_0}{p} \right) \text{ m.}$$

1164 It follows that the Curvature-redshift will not be in-
1165 hibited if $X < L$ or in this case, the pressure is less than
1166 $0.0014p_0$ which is about 1 mm of Hg. For this pressure,
1167 we find that $X = 57$ m which requires that the appa-
1168 ratus must be much longer than 57 m. For argument
1169 let us take the length to be 100 m then the fractional
1170 redshift expected is 2.1×10^{-13} which is detectable.

1171 The experimental method would use a horizontal (to
1172 eliminate gravitational redshifts) tube filled with helium
1173 and with accurately controlled temperature. Then we
1174 would measure the redshift as a function of pressure.
1175 The above theory predicts that if it is free of inhibition
1176 then the redshift should be proportional to the square
1177 root of the pressure.

1178 Alternatively, it may be possible to detect the sec-
1179 ondary photons. For helium with a pressure of 1 mm
1180 Hg the expected frequency of the secondary radiation
1181 from ^{57}Fe is about 100 kHz. The expected power from
1182 a 1 Cu source is about 5×10^{-22} W. Unfortunately, the
1183 secondary radiation could be spread over a fairly wide
1184 frequency band which makes its detection somewhat dif-
1185 ficult but it may be possible to detect the radiation with
1186 modulation techniques.

1187 4. PART C: OBSERVATIONS

1188 4.1. *Type Ia supernova*

1189 For the 1,652 Type Ia supernova analyzed in Part A
1190 the light curve width is

$$w_{obs}(z) = 1.060 \pm 0.009 + (1.080 \pm 0.042) z. \quad (37)$$

1191 and the regression of the absolute magnitudes as a func-
1192 tion of redshift is

$$M(z) = -17.597 \pm 0.012 + (0.143 \pm 0.057) z,$$

1193 Both results shows very strong support for Curvature-
1194 cosmology.

1195 4.2. *X-ray background radiation*

1196 since [Giacconi et al. \(1962\)](#) observed the X-ray back-
1197 ground there have been many suggestions made to ex-
1198 plain its characteristics. Although much of the unre-
1199 solved X-ray emission comes from active galaxies, there
1200 is a part of the spectrum between about 10 keV and 1
1201 MeV that is not adequately explained by emission from
1202 discrete sources. The very high energy range is most
1203 likely due to external point sources. It is the interme-
1204 diate range that is examined here.

1205 In Λ CDM cosmology for the intermediate X-ray range
1206 of about 10–300 keV, the production of X-rays in hot
1207 cosmic plasma through the process of bremsstrahlung
1208 has been suggested by [Hoyle \(1962\)](#); [Gould & Bur-
1209 bidge \(1963\)](#); [Field & Henry \(1964\)](#); [Cowsik & Kobetich
1210 \(1972\)](#).

1211 In a review of the spectrum of the X-ray background
1212 radiation [Holt \(1992\)](#) concluded that the measured spec-
1213 tra of discrete sources are not consistent with the obser-
1214 vations in the intermediate energy range but there is a
1215 remarkable fit to a 40 keV (4.6×10^8 K) bremsstrahlung
1216 spectrum from a diffuse hot gas.

1217 However, in an expanding universe most of the X-
1218 rays are produced at redshifts of $z \approx 3$ where the den-
1219 sity is large enough to scatter the CMBR. This scat-
1220 tering known as the Sunyaev–Zel’dovich effect (see Sec-
1221 tion 4.12) makes a distinct change in the spectrum of
1222 the CMBR. This predicted change in the spectrum has
1223 not been observed and this is the major reason why the
1224 bremsstrahlung model in Λ CDM is rejected.

1225 In Curvature-cosmology, the basic component of the
1226 universe is plasma with a very high temperature,
1227 and with low enough density to avoid the Sunyaev–
1228 Zel’dovich effect.

1229 The background X-ray emission is produced in
1230 this plasma by the process of free-free emission
1231 (bremsstrahlung). The observations of the background
1232 X-ray emission are analyzed in order to measure the
1233 density and temperature of the plasma. In Curvature-
1234 cosmology, this density is the major free parameter and

it determines the size of the universe and the value of the Hubble constant.

In addition, the temperature of the plasma determined from the X-ray measurements can be compared with the predicted value from Curvature-cosmology for pure hydrogen of 2.456×10^9 K.

The first step is to calculate the expected X-ray emission from high temperature plasma in thermal equilibrium. Here the dominant mechanism is bremsstrahlung radiation from electron-ion and electron-electron collisions. With a temperature T and emission into the frequency range ν to $\nu + d\nu$ the volume emissivity per steradian can be written as

$$j_\nu(\nu)d\nu = \left(\frac{16}{3}\right) \left(\frac{\pi}{6}\right)^{1/2} r_0^3 m_e c^2 \left(\frac{m_e c^2}{kT}\right)^{1/2} \times g(\nu, T) \exp\left(-\frac{h\nu}{kT}\right) N_e \sum Z_i^2 N_i d\nu, \quad (38)$$

where $g(\nu, T)$ is the Gaunt factor, N_e is the electron number density, N_i is the ion number density and r_0 is the classical electron radius and the other symbols have their usual significance (Nozawa, Itoh, & Kohyama 1998). The intensity, $j_\nu(\nu)$, has the units of $\text{W m}^{-3} \text{Hz}^{-1}$.

As it stands this equation does not include the electron-electron contribution. Nozawa et al. (1998) and Itoh et al. (2000) have done accurate calculations for many light elements. Based on their calculations Professor Naoki Itoh (<http://www.ph.sophia.ac.jp/>) provides a subroutine to calculate the Gaunt factor that is accurate for temperatures greater than 3×10^8 K. It is used here.

Because of the very high temperature, we can assume that all atoms are completely ionized. Thus, Eq. 38 including the Gaunt factor provides the production rate of X-ray photons as a function of the plasma temperature and density.

The next step is to compute the expected intensity at an X-ray detector. Consider an X-ray photon that is produced at a distance $R\chi$ from the detector. During its travel to the detector, it will have many Curvature-redshift interactions. Although the photon is destroyed in each interaction, there is a secondary photon produced that has the same direction but with a slightly reduced energy.

It is convenient to consider this sequence of photons as a single particle and to refer to it as a primary photon. The important result is that the number of these primary photons is conserved. Therefore, we need the production distribution of the number of photons per unit energy interval. The number of photons emitted per unit volume per unit time in the energy interval ε

to $\varepsilon + d\varepsilon$ is given by

$$j_n(\varepsilon) d\varepsilon = \frac{j_\nu(\nu)}{\varepsilon} h d\nu, \quad (39)$$

where $\varepsilon = h\nu$, h is Plank's constant and $j_\nu(\nu)$ is the energy distribution per unit frequency interval.

Now consider the contribution to the number of X-rays observed by a detector with unit area. Because the universe is static, the area at a distance R from the source is the same as the area at a distance R from the detector. Since there is conservation of these photons, the number coming from a shell at radius R per unit time and per steradian within the energy interval ε to $\varepsilon + d\varepsilon$ is

$$\frac{dn(r)}{dt} d\varepsilon = j_n(\varepsilon) d\varepsilon R d\chi.$$

Next, we integrate the photon rate per unit area and per steradian from each shell where the emission energy is ε and the received energy is ε_0 to get

$$I_n(\varepsilon_0) d\varepsilon_0 = R \int_0^{\chi_m} j_n(\varepsilon) d\varepsilon d\chi,$$

where $\varepsilon = (1+z)\varepsilon_0$ and it is assumed that the flux is uniform over the 4π steradian. Furthermore, it is useful to change the independent coordinate to the redshift parameter z .

Then using Eq. 39 we get

$$I_\nu(\nu_0) d\nu_0 = \frac{c}{H} \int_0^{z_m} \frac{j_\nu(\nu)}{1+z} dz d\nu_0,$$

where H is the Hubble constant and the change in bandwidth factor $d\nu/d\nu_0$, cancels the $(1+z)$ factor that comes from the change in variable from $d\chi$ to dz but there is another divisor of $(1+z)$ that accounts for the energy lost by each photon.

Thus the energy flux per unit area, per unit energy interval, per unit frequency and per solid angle is given by Eq. 40 where Plank's constant is included to change the differential from frequency to energy. The z_m limit of 8.2 comes from the limit of $\chi \leq \pi$.

$$\begin{aligned} I_\nu(\nu_0) &= \left(\frac{16}{3}\right) \left(\frac{\pi}{6}\right)^{1/2} \frac{r_0^3 m_e c^3}{h} (8\pi GM_H)^{-1/2} \left(\frac{m_e c^2}{kT}\right)^{1/2} \\ &\times n_e n_i N_e^{3/2} \int_0^{z_m} \frac{g((1+z)\nu_0, T)}{(1+z)} \exp\left(-\frac{h(1+z)\nu_0}{kT}\right) dz \\ &= \frac{1.9094 \times 10^3 \text{ keV}}{\text{keV m}^2 \text{ s sr}} \left(\frac{m_e c^2}{kT}\right)^{1/2} n_e n_i N_e^{3/2} \\ &\times \varepsilon_0 \int_0^{z_m} \frac{g((1+z)\nu_0, T)}{(1+z)} \exp\left(-\frac{h(1+z)\nu_0}{kT}\right) dz. \quad (40) \end{aligned}$$

Table 3. List of background X-ray data used.

Name	Instrument	Reference
Gruber	HEAO 1 A-4	Gruber et al. (1999)
Kinzer	HEAO 1 MED	Kinzer et al. (1997)
Dennis	OSO-5	Dennis et al. (1973)
Mazets	Kosmos 541	Mazets et al. (1975)
Mandrou	Balloon	Mandrou et al. (1979)
Trombka	Apollo 16, 17	Trombka et al. (1977)
Santalogo	Rocket	Santangelo et al. (1973)
Fukada	Rocket	Fukada et al. (1975)

Table 4. Background X-ray data: rejected points.

Source	Energy keV	Flux density keV/(keV cm ² s sr)	χ^2 (1 DoF)
Gruber	98.8	0.230±0.012	108.6
Gruber	119.6	0.216±0.022	65.2
Fukada	110.5	0.219±0.011	66.6
Gruber	152.6	0.140±0.022	50.9
Fukada	179.8	0.110±0.005	41.5
Gruber	63.9	0.484±0.034	25.1

1311 The density N_ϵ is obtained by fitting Eq. 40 to the
 1312 observed data as a function of the temperature T , and
 1313 then extracting N_ϵ from the normalization constant.

1314 The X-ray data used is tabulated in Table 3. It con-
 1315 sists of the background X-ray data cited in the literature
 1316 and assessed as being the latest or more accurate results.
 1317 Preliminary analysis showed that there were some dis-
 1318 crepant data points that are listed in Table 4 in order of
 1319 exclusion.

1320 Very hard X-rays cannot be produced even by this hot
 1321 plasma and are presumably due to discrete sources (Holt
 1322 1992).

1323 The results of the fit of the data to this model of pure
 1324 hydrogen is a temperature of

$$(2.62 \pm 0.13) \times 10^9 \text{ K}, \quad (41)$$

1325 which is good agreement with the predicted temperature
 1326 of $2.456 \times 10^9 \text{ K}$.

1327 The measured density is

$$1.93 \pm 0.13 \text{ H atoms per m}^3, \quad (42)$$

1328 which is the only free parameter in Curvature-
 1329 cosmology.

1330 Most of the X-ray flux below 10 keV and part of the
 1331 flux just above 10 keV is emission from discrete sources.
 1332 The deviation from the curve at energies above about
 1333 300 keV arises from X-rays coming from discrete sources.

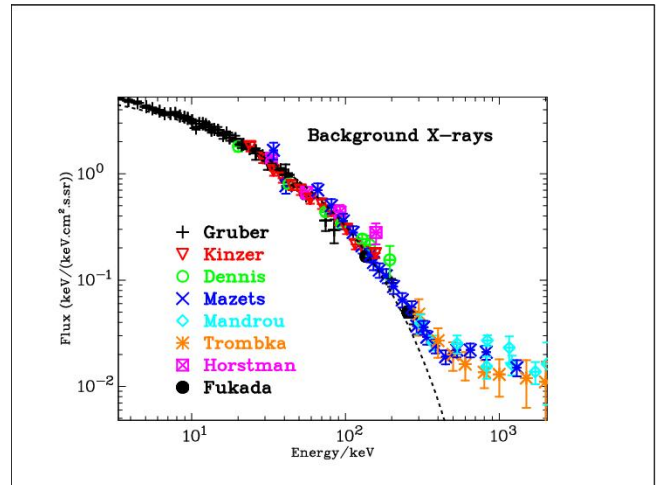


Figure 5. Background X-ray spectrum. See Table 3 for list of observations. The dashed (black) line is best fit from 10 keV to 300 keV for the pure hydrogen model.

1334 In the intermediate region where bremsstrahlung
 1335 should dominate, there are clear signs of some minor
 1336 systematic errors. In addition, there appears to be some
 1337 variation between the data sets. It is not clear whether
 1338 the discrepancy between the observed points and the
 1339 predicted flux densities is due to an inadequate theory,
 1340 inadequate X-ray emission model, or systematic errors
 1341 in the observations. After all the measurements are very
 1342 difficult and come from a wide range of rocket, bal-
 1343 loon and satellite experiments. In particular, the recent
 1344 HEAO results Kinzer et al. (1997) differ from earlier
 1345 results reported by Marshall et al. (1980).

1346 In Curvature-cosmology, the argument against
 1347 bremsstrahlung based on the Sunyaev–Zel’dovich effect
 1348 is not valid because the density of the gas is much less
 1349 and the CMBR has a different source.

4.3. Cosmic microwave background radiation.

1350 The cosmic microwave background radiation (CMBR)
 1351 is one of the major success stories for the standard model
 1352 . The observed radiation has a spectrum that is ex-
 1353 tremely close to a black body spectrum which means
 1354 that it can be described by a single parameter, its tem-
 1355 perature.

1356 Observations of the CMBR spectrum were obtained
 1357 from the FIRAS instrument on the *Cobe* satellite by
 1358 Mather et al. (1990). They measured the temperature of
 1359 the CMBR to be 2.725 K. This temperature is in agree-
 1360 ment with the observations of Roth & Meyer (1995) who
 1361 measured a temperature of 2.729(+0.023, −0.031) K us-
 1362 ing cyanogen excitation in diffuse interstellar clouds.
 1363 More recently Fixsen (2009) using data from the Wilkin-
 1364 son Microwave Anisotropy Probe (WMAP) and many
 1365

1366 earlier results provide a temperature of $2.72548 \pm$
1367 0.00057K .

1368 The theoretical value from Curvature-cosmology is
1369 2.736 which is within 0.4% but well outside the WMAP
1370 uncertainty. However there is a fundamental difference
1371 between the two values in that the standard model as-
1372 sumes that the CMBR arose just after the big bang and
1373 has been redshifted to its current value. That is the
1374 observed value will have radiation from distances with
1375 presumed higher redsifts. Whether this can explain the
1376 small discrepancy depends on details of the analysis.

1377 4.4. Tolman surface .

1378 This test, suggested by Tolman (1934), relies on the
1379 observation that the surface brightness of objects does
1380 not depend on the geometry of the universe. Although
1381 it is obviously true for Euclidean geometry, it is also true
1382 for non-Euclidean geometries. For a uniform source, the
1383 quantity of light received per unit angular area is in-
1384 dependent of distance. However, the quantity of light
1385 is also sensitive to non-geometric effects, which make
1386 it an excellent test to distinguish between cosmologies.
1387 For expanding universe cosmologies the surface bright-
1388 ness is predicted to vary as $(1+z)^{-4}$, where one factor of
1389 $(1+z)$ comes from the decrease in energy of each photon
1390 due to the redshift, another factor comes from the de-
1391 crease in the rate of their arrival and two factors come
1392 from the apparent decrease in area due to aberration.
1393 This aberration is simply the rate of change of area for
1394 a fixed solid angle with redshift. In a static, tired-light,
1395 cosmology (such as Curvature-cosmology) only the first
1396 factor is present. Thus an appropriate test for Tolman
1397 surface brightness is the value of this exponent.

1398 The obvious candidates for surface brightness tests are
1399 elliptic and S0 galaxies which have minimal projection
1400 effects compared to spiral galaxies . The major problem
1401 is that surface brightness measurements are intrinsically
1402 difficult due to the strong intensity gradients across their
1403 images. In a series of papers Sandage & Lubin (2001);
1404 Lubin & Sandage (2001a,b,c) (hereafter SL01) have in-
1405 vestigated the Tolman surface brightness test for ellipti-
1406 cal and S0 galaxies. More recently Sandage (2010) has
1407 done a more comprehensive analysis but since he came
1408 to the same conclusion as the earlier papers and since
1409 the earlier papers are better known this analysis will
1410 concentrate on them.

1411 The observational difficulties are thoroughly discussed
1412 by Sandage & Lubin (2001) with the conclusion that
1413 the use of Petrosian metric radii helps solve many of
1414 the problems. Petrosian (1976); Djorgovski & Spinrad
1415 (1981); Sandage & Perelmuter (1990) showed that if the
1416 ratio of the average surface brightness within a radius

Table 5. Galactic properties for Petrosian radius $\eta = 2.0$

Cluster	N	$\overline{\log(S_{BB})}$	$\overline{m_{BB}}$	$\overline{M_{BB}}$
Nearby	74	4.69 ± 0.28	22.56 ± 0.84	-23.84 ± 0.66
1324+3011	11	3.99 ± 0.21	22.87 ± 0.75	-23.28 ± 0.65
1604+4304	6	4.05 ± 0.17	22.34 ± 0.60	-23.51 ± 0.68
1604+4321	13	4.00 ± 0.15	22.35 ± 0.78	-23.33 ± 0.64

1417 is equal to η times the surface brightness at that radius
1418 then that defines the Petrosian metric radius, η . The
1419 procedure is to examine an image and to vary the angu-
1420 lar radius until the specified Petrosian radius is achieved.

1421 Thus, the aim is to measure the mean surface bright-
1422 ness for each galaxy at the same value of η . The choice of
1423 Petrosian radii greatly diminishes the differences in sur-
1424 face brightness due to the luminosity distribution across
1425 the galaxies. However, there still is a dependence of the
1426 surface brightness on the size of the galaxy which is the
1427 Kormendy relationship (Kormendy 1977).

1428 The purpose of the preliminary analysis done by SL01
1429 is not only to determine the low redshift absolute lu-
1430 minosity but also to determine the surface brightness
1431 verses linear size relationship that can be used to cor-
1432 rect for effects of size variation in distant galaxies. The
1433 data on the nearby galaxies used by SL01 was taken
1434 from Postman & Lauer (1995) and consists of extensive
1435 data on the brightest cluster galaxies (BCG) from 119
1436 nearby Abell clusters. All magnitudes for these galaxies
1437 are in the R_C (Cape/Landolt) system.

1438 Since the results for different Petrosian radii are highly
1439 correlated the analysis repeated here using similar pro-
1440 cedures will use only the Petrosian $\eta = 2$ radius. Al-
1441 though the actual value used for h does not alter any
1442 significant results here, it is set to $h = 0.5$ for numer-
1443 ical consistency. A minor difference is that the angu-
1444 lar radius used here is provided by Curvature-cosmology
1445 whereas they used the older Mattig equation.

1446 The higher z data also comes from SL01. They made
1447 Hubble Space Telescope observations of galaxies in three
1448 clusters and measured their surface brightness and radii.
1449 The names and redshifts of these clusters are given in
1450 Table 5 which also shows the number of galaxies in each
1451 cluster, N , the logarithm of the average metric radius
1452 in kpc, $\log(S_{BB})$, and the average apparent magnitude
1453 and the absolute magnitude. In order to avoid confusion
1454 in BB denotes a measurement made using the standard
1455 Λ CDM cosmology. Note that the original magnitudes
1456 for Cl 1324+3011 and Cl 1604+4304 were observed in
1457 the I band.

1458 In order to get a reference surface brightness at $z = 0$
1459 all the surface brightness values, SB, of the nearby galax-

ies were reduced to absolute surface brightness by using Eq. 43. Since all the redshifts are small, this reduction is essentially identical for all cosmological models. However the calculation of the metric radii for the distant galaxies is very dependent on the cosmological model.

This procedure of using the same cosmology in analyzing a test of that cosmology is discussed in SL01. Their conclusion is that it reduces the significance of a positive result from being *strongly supportive* to being *consistent with the model*. Of interest is that Table 5 shows that on average the distant galaxies are fainter than the nearby galaxies.

Then a linear least squares fit of the absolute surface brightness as a function of $\log(S_{BB})$, the Kormendy relationship, for the nearby galaxies results in the equation

$$SB = 9.29 \pm 0.50 + (2.83 \pm 0.11) \log(S_{BB}) \quad (43)$$

whereas SL01 found the slightly different equation

$$SB = 8.69 \pm 0.06 + (2.97 \pm 0.05) \log(S_{BB}). \quad (44)$$

Although a small part of the discrepancy is due to slightly different procedures, the main reason for the discrepancy is unknown. Of the 74 galaxies used, there were 19 that had extrapolated estimates for either the radius or the surface brightness or both. In addition there were only three galaxies that differed from the straight line by more than 2σ . They were A147 (2.9σ), A1016 (2.0σ) and A3565 (-2.4σ). Omission of all or some of these galaxies did not improve the agreement. The importance of this preliminary analysis is that Eq. 43 contains all the information that is needed from the nearby galaxies in order to calibrate the distant cluster galaxies.

Next we use the galaxies' radius and Eq. 43 to correct the apparent surface brightness of the distant galaxies for the Kormendy relation and then do least squares fit to the difference between the corrected surface brightness and its absolute surface brightness as a function of $2.5 \log(1+z)$ to estimate the exponent, n , where $SB \propto (1+z)^n$. If needed the non-linear corrections given by Sandage (2010) were applied to the nearby surface brightness values. For the I band galaxies, the absolute surface brightness included the color correction $< R - I > = 0.62$ Lubin & Sandage (2001c).

The results for the exponent, n , for each cluster are shown in Table 6 together with the values from SL01 (column 5) where the second column is the band (color) in which the cluster was observed.

Because the definition of magnitude contains a negative sign the expected value for n in BB is four. Nearly all of the difference between these results and those from

Table 6. Fitted exponents for distant clusters ($\eta = 2.0$)

Cluster	Col	\bar{z}	n_{BB}	n_{SL01}
1324+3011	I	0.757	1.98 ± 0.19	1.99 ± 0.15
1604+4304	I	0.897	2.22 ± 0.22	2.29 ± 0.21
1604+4321	R	0.924	2.24 ± 0.18	2.48 ± 0.25

SL01 arise from the use of a different Kormendy relationship. If the Kormendy relationship used by SL01 Eq. 44 is used instead of Eq. 43) the agreement is excellent. If it is assumed that there is no evolutionary or other differences between the three clusters and all the data are combined the resulting exponent is $n_{BB} = 2.16 \pm 0.13$.

Clearly, there is a highly significant disagreement between the observed exponents and the expected exponent of four. Both SL01 and Sandage (2010) claim that the difference is due to the effects of luminosity evolution. Based on a range of theoretical models SL01 show that the amount of luminosity evolution expressed as the exponent, $p = 4 - n_{BB}$, varies between $p = 0.85 - 2.36$ in the R band and $p = 0.76 - 2.07$ in the I band. In conclusion, to their analysis, they assert that *they have either (1) detected the evolutionary brightening directly from the SB observations on the assumption that the Tolman effect exists or (2) confirmed that the Tolman test for the reality of the expansion is positive, provided that the theoretical luminosity correction for evolution is real.*

SL01 also claim that their results are completely inconsistent with a tired light cosmology. Although this is explored for Curvature-cosmology in the next subsection, it is interesting to consider a very simple model. The essential property of a tired light model is that it does not include the time dilation factor of $(1+z)$ in its angular radius equation. Thus assuming BB but without the $(1+z)$ term all values of $\log(S_{BB})$ will be increased by $\log(1+z)$. Hence the predicted absolute surface brightness will be (numerically) increased by $(2.83/2.5)\log(1+z)$. For example, the exponent for all clusters will be changed to

$$n_{\text{tired_light}} = 2.16 \pm 0.16 - \frac{2.83}{2.5} = 1.03 \pm 0.16$$

This is clearly close to the expected value of unity predicted by a tired-light cosmology and thus disagrees with the conclusion of SL01 that the data are incompatible with a tired light cosmology.

There are two major criticisms of this work. The first is that relying on theoretical models to cover a large gap between the expected index and the measured index makes the argument very weak. Although SL01 indirectly consider the effects of relatively common galaxy

Table 7. Radii and fitted exponents for distant clusters ($\eta = 2.0$)

Cluster	N	$\log(\bar{S})$	\bar{M}	n
nearby	74	4.70 ± 0.28	-23.78 ± 0.66	
1324+3011	11	4.18 ± 0.21	-22.41 ± 0.66	1.19 ± 0.19
1604+4304	6	4.27 ± 0.17	-22.54 ± 0.65	1.45 ± 0.21
1604+4321	13	4.23 ± 0.15	-22.33 ± 0.68	1.48 ± 0.17

interactions and mergers in the very wide estimates they provide for the evolution, the fact that there is such a wide spread makes the argument that Tolman surface brightness for this data is consistent with Λ CDM possible but weak.

Ideally, there would be an independent estimate of p based on other observations. The second criticism is that the nearby galaxies are not the same as the distant cluster galaxies. The nearby galaxies are all brightest cluster galaxies (BCG) whereas the distant cluster galaxies are normal cluster galaxies. It is well known that BCG (Blanton & Moustakas 2009) are in general much brighter and larger than would be expected for the largest member of a normal cluster of galaxies. Whether or not this amounts to a significant variation is unknown but it does violate the basic rule that like should be compared with like.

Unsurprisingly it is found that using Curvature-cosmology the relationship between absolute surface brightness and radius is identical to that shown in Table 5. What is different is the average radius, the absolute magnitudes and the observed exponent n . These are shown in Table 7.

The result for all clusters is $n = 1.38 \pm 0.13$ which is in agreement with unity. Note that the critical difference from the standard analysis is in the size of the radii. They are not only much closer to the nearby galaxy radii but because they are larger they do not require the non-linear corrections for the Kormendy relation. As before we note that the nearby galaxies are BCG which may have a brighter SB than the normal field galaxies. If this is true, it would bias the exponent to a larger value. If we assume that Curvature-cosmology is correct then this data shows that on average the BCG galaxies are -0.64 ± 0.08 mag (which is a factor of 1.8 in luminosity) brighter than the general cluster galaxies.

The SL01 data for the surface brightness of elliptic galaxies is consistent with Λ CDM but only if a large unknown effect of luminosity evolution is included. The data do not support expansion and are in complete agreement with Curvature-cosmology.

4.5. Dark matter and Coma cluster

All observational evidence for dark matter comes from the application of Newtonian gravitational physics to either clusters of objects or the rotation of galaxies. Galaxy rotation will be dealt with in Section 4.20. The original concept for dark matter comes from applying the virial theorem to the Coma cluster of galaxies (Zwicky 1937). The virial theorem is a statistical theorem that states that for an inverse square law the average kinetic energy of a bound system is equal to half the potential energy (i.e. $2T + V = 0$).

Then with knowing the linear size of the cluster and measuring the mean square spread of velocities we can estimate the total mass of the cluster. There is no doubt that applying the virial theorem to the Coma and other clusters of galaxies provides mass estimates that can be several hundred times the mass expected from the total luminosity. Even the mass of intergalactic gas is not enough to overcome this imbalance. In Λ CDM cosmology dark matter has been introduced to make up for the shortfall of mass.

However if Curvature-cosmology is valid then it is possible that the observed redshifts are not due to kinematic velocities but are Curvature-redshifts produced by the intergalactic gas. The purpose of this section is to show that Curvature-redshift can explain the galactic velocities without requiring dark matter.

For simplicity, we will use the Coma cluster as a test bed. Not only is it very well studied, but it also has a high degree of symmetry and the presence of an intergalactic gas cloud is known from X-ray observations. Watt et al. (1992) and Hughes (1989) have fitted the density of the gas cloud to an isothermal model with the form

$$\rho = \rho_0 \left(1 + \left(\frac{r}{r_e}\right)\right)^{-\alpha}, \quad (45)$$

with a center at $12^h 59^m 10^s, 27^\circ 59' 56''$ (J2000) and with $r_e = 8.8' \pm 0.7'$, $\alpha = 1.37 \pm 0.09$, $\rho_0 = (2.67 \pm 0.22) \times 10^3 N_\epsilon$. The central density is obtained from the X-ray luminosity and has a strong dependence on the distance. Watt et al. (1992) assumed a Hubble constant of $50 \text{ km s}^{-1} \text{ Mpc}^{-1}$. With a mean velocity of $6,853 \text{ km s}^{-1}$ (Colless & Dunn 1996) and with this Hubble constant, the distance to the Coma cluster is 137 Mpc. Recently Rood (1988) using the Tully–Fisher relation to measure the distance modulus to the galaxies in the Coma cluster, to observe a value of 34.4 ± 0.2 mag whereas Liu & Graham (2001) using infrared surface brightness fluctuations get 34.99 ± 0.21 mag. The average is 34.7 mag that corresponds to a distance of 87.1 Mpc. This is consistent with the distance of 85.6 Mpc given by Freedman et al. (2001).

Table 8. Coma velocity dispersions for some distances.

Distance/Mpc	50	87	100	150
Dispersion /km s ⁻¹	318	554	636	955

The galactic velocity data are taken from [Beijersbergen \(2003\)](#) who provide information for 583 galaxies. The velocity centroid of the Coma cluster is $12^h59^m19^s$, $27^\circ52'2''$ (J2000). They find that early-type galaxies (E+S0+E/S0) have a mean velocity of $9,926 \text{ km s}^{-1}$ and a rms (root-mean-square) velocity, of 893 km s^{-1} . Let us assume that all the galactic velocities are due to Curvature-redshift. That is we assume that the actual velocities, the peculiar velocities, are negligible. Then the redshifts for the galaxies are calculated (in velocity units) by

$$v = v_0 + \int_0^Z 51.691 \sqrt{N(Z)} dZ \text{ km s}^{-1}, \quad (46)$$

where Z is the distance from the central plane of the Coma cluster to the galaxy measured in Mpc, $N(Z)$ is the density of the intergalactic gas cloud and v_0 is the average velocity of the galaxies in the cluster. The problem here is that we do not know Z distances. Nevertheless, we can still get a good estimate by assuming that the distribution in Z is statistically identical to that in X and in Y . In a Monte Carlo simulation, each galaxy was given a Z distance that was the same as the X (or Y) distance of one of the other galaxies in the sample chosen at random. For 50 trials, the computed dispersion was 554 km s^{-1} which can be compared with the measured dispersion of 893 km s^{-1} . Curvature-cosmology has predicted the observed dispersion of galactic velocities in the Coma cluster to within a factor of two.

Considering that this is a prediction of the cosmological model without fitting any parameters and ignoring all the complications of the structure both in the gas and galactic distributions the agreement is remarkable.

Since the distance to the Coma cluster is an important variable, the computed velocity dispersion from the Monte Carlo simulation for some different distances (all the other parameters are the same) is shown in [Table 8](#). Thus, the redshift dispersion (in velocity units) is approximately a linear function of the Coma distance. This is not surprising since in this context the distance is mainly a scale factor.

[Beijersbergen \(2003\)](#) note that a better fit to the velocity distribution is provided by the sum of two Gaussian curves. Their best fit parameters for these two Gaussians are $v_1 = 7,501 \pm 187 \text{ km s}^{-1}$, with $\sigma_1 = 650 \pm 216 \text{ km s}^{-1}$ and $v_2 = 6641 \pm 470 \text{ km s}^{-1}$, with $\sigma_2 = 1,004 \pm 120 \text{ km s}^{-1}$. This double structure is sup-

ported by [Colless & Dunn \(1996\)](#) who argue for an on-going merger between two sub clusters centered in projection on the dominant galaxies NGC 4874 and NGC 4889.

In addition, [Briel, Henry, & Boehringer \(1992\)](#) found evidence for substructure in the X-ray emission and [Finoguenov et al. \(2004\)](#) and [White, Briel, & Henry \(1993\)](#) have measured the X-ray luminosity of individual galaxies in the Coma cluster showing that the model for the gas used above is too simple. The net effect of this substructure is that the observed velocity dispersion would be different from that predicted by a simple symmetric model. Thus, it appears that substructure makes it very difficult to achieve a more accurate test of Curvature-cosmology using the Coma cluster.

There is an important difference between Curvature-redshift and models that assume that the redshifts of the galaxies within a cluster are due to their velocities. Since the laws of celestial mechanics are symmetric in time, any galaxy could equally likely be going in the opposite direction. Thus a galaxy with a high relative (Z) velocity could be in the near side of the cluster or equally likely on the far side of the cluster. However, if the redshifts are determined by Curvature-redshift then there will be a strong correlation in that the higher redshifts will come from galaxies on the far side of the cluster.

A possible test is to see if the apparent magnitudes are a function of relative redshift. With a distance of 87.1 Mpc the required change in magnitude is about $0.025 \text{ mag Mpc}^{-1}$. A simple regression between magnitude of Coma galaxies (each relative to its type average) and velocity did not show any significant dependence.

Although this was disappointing, several factors can explain the null result. The first is the presence of the substructure; the second is that the magnitudes for a given galactic type have a standard deviation of about one magnitude, which in itself is sufficient to wash out the predicted effect; and thirdly mistyping will produce erroneous magnitudes due to the different average velocities of different types. In support of the second factor, we note that for 335 galaxies with known types and magnitudes, the standard deviation of the magnitude is 1.08 mag and if we assume that the variance of the Z distribution is equal to the average of the variances for the X and Y distributions then the expected standard deviation of the slope is $0.076 \text{ mag Mpc}^{-1}$. Clearly, this is such larger than the expected result of $0.025 \text{ mag Mpc}^{-1}$. It is expected that better measurements or new techniques of measuring differential distances will in the future make this a very important cosmological test.

In Λ CDM observations of the velocity dispersion of clusters of galaxies cannot be explained without invok-

ing an ad hoc premise such as dark matter. However Curvature-cosmology not only explains the observations but also makes a good prediction, without any free parameters, of its numerical value.

4.6. Angular size

Closely related to surface brightness is relationship between the observed angular size of a distant object and its actual linear transverse size.

The major distinction in angular size is that Curvature-cosmology, like all tired-light cosmologies, does not include the $(1+z)$ aberration factor. Its relationship between the observed angular size and the linear size is very close (for small redshifts) to the Euclidean equation.

Gurvits, Kellermann, & Frey (1999) provide a comprehensive history of studies for a wide range of objects that generally show a $1/z$ or Euclidean dependence. Most observers suggest that the probable cause is some form of size evolution. Recently López-Corredoira (2010) used 393 galaxies with redshift range of $0.2 < z < 3.2$ in order to test many cosmologies.

Briefly, his conclusions are

The average angular size of galaxies is approximately proportional to $z^{-\alpha}$ with α between 0.7 and 1.2.

Any model of an expanding universe without evolution is totally unable to fit the angular size data ...

Static Euclidean models with a linear Hubble law or simple tired-light fit the shape of the angular size vs z dependence very well: there is a difference in amplitude of 20%–30%, which is within the possible systematic errors.

It is also remarkable that the explanation of the test results with an expanding model require four coincidences:

- 1. The combination of expansion and (very strong evolution) size evolution gives nearly the same result as a static Euclidean universe with a linear Hubble law: $\theta \propto z^{-1}$.*

- 2. This hypothetical evolution in size for galaxies is the same in normal galaxies as in quasars, as in radio galaxies, as in first ranked cluster galaxies, as the separation among bright galaxies in cluster*

- 3. The concordance model gives approximately the same (differences of less than 0.2 mag within $z < 4.5$) distance modulus in a Hubble diagram as the static Euclidean universe with a linear law.*

- 4. The combination of expansion, (very strong) size evolution, and dark matter ratio variation gives the same result for the velocity dispersion in elliptical galaxies (the result is that it is nearly constant with z) as for a simple static model with no evolution in size and no dark matter ratio variation.*

With a redshift range of $z < 3$ the value of S is approximately proportional to $z^{0.68}$ which shows that it is consistent with these results. A full analysis requires a fairly complicated procedure to correct the observed sizes for variations in the absolute luminosity.

A simple example of the angular size test can be done using double-lobed quasars. Using quasar catalogues, Buchalter et al. (1998) carefully selected 103 edge-brightened, double-lobed sources from the VLA FIRST survey and measured their angular sizes directly from the FIRST radio maps.

Since Buchalter et al. (1998) claim that three different Friedmann Λ CDM models fit the data well but that a Euclidean model had a relatively poor fit a reanalysis is warranted.

Their angular sizes were converted to linear sizes for each cosmology and were divided into six bins so that there were 17 quasars in each bin. Because these double-lobed sources are essentially one-dimensional a major part of their variation in size is due to projection effects.

For the moment assume that in each bin they have the same size, \hat{S} , and the only variation is due to projection then the observed size is $\hat{S} \sin(\theta)$ where θ is the projection angle. Clearly, we do not know the projection angle but we can assume that all angles are equally likely so that if the N sources, in each bin, are sorted into increasing size the i 'th source in this list should have, on average, an angle $\theta_i = \pi(2i-1)/4N$. Thus the maximum likelihood estimate of \hat{S} is

$$\hat{S}_{\text{est}} = \frac{\sum_{i=1}^N \sin(\theta_i) S_i}{\sum_{i=1}^N \sin^2(\theta_i)}.$$

Note that the sum in the denominator is a constant and that the common procedure of using median values is the same as using only the central term in the sum.

Next a regression was done between logarithm of the estimated linear size in each bin and $\log(1+z)$ where z is the mean redshift. Then the significance of the test was how close was the exponent, b , to zero. For Λ CDM the exponent was $b = -0.79 \pm 0.44$ and for Curvature-cosmology, it was $b = 0.16 \pm 0.44$. Although the large uncertainties show that this is not a decisive discrimination between the two cosmologies the slope for the Curvature-cosmology suggests that no expansion is more likely.

1832 For angular size the conclusion is in favor of
1833 Curvature-cosmology.

1834 *4.7. Galaxy distribution*

1835 Recently, large telescopes with wide fields and the
1836 use of many filters have enabled a new type of galac-
1837 tic survey. The light-collecting capability of the large
1838 telescopes enables deep surveys to apparent magnitudes
1839 of 24 mag or better and the wide field provides a fast
1840 survey over large areas.

1841 A major innovation is the use of many filters whose
1842 response can be used to classify the objects with great
1843 accuracy. Thus, galaxies can be separated from quasars
1844 without needing morphological analysis. This photo-
1845 metric method of analysis works because photometric
1846 templates are available for a wide range of types of galax-
1847 ies and other types of objects. In addition, accurate
1848 redshifts are obtained from fitting the templates with-
1849 out the tedious procedure of measuring the spectrum of
1850 each object.

1851 A typical example of this photometric method is the
1852 COMBO-17 survey (Classifying Objects by Medium-
1853 Band Observations in 17 filters) provided by [Wolf et al.](#)
1854 (2004). The goal of this survey was to provide a sample
1855 of 50,000 galaxies and 1000 quasars with rather precise
1856 photometric redshifts based on 17 colors.

1857 In practice, such a filter set provides a redshift accu-
1858 racy of 0.03 for galaxies and 0.1 for quasars. The
1859 central wavelength of the 17 filters varied from 364
1860 nm to 914 nm and consisted of 5 broadband filters
1861 (*U, B, V, R, I*) and 12 narrower-band filters. [Wolf et al.](#)
1862 (2003) have analyzed this data and claim that there is
1863 strong evolution for $0.2 < z < 1.2$.

1864 Instead of using generic K-corrections, the intrinsic
1865 (rest frame) luminosity of all galaxies are individually
1866 measured from their 17-filter spectrum. For each galaxy,
1867 three rest-frame pass bands are considered, (i) the SDSS
1868 *r*-band, (ii) the Johnston *B*-band and (iii) a synthetic
1869 UV continuum band centered at $\lambda_{rest} = 280$ nm with 40
1870 nm FWHM and rectangular transmission function.

1871 A spectral energy distribution, SED, was determined
1872 for each galaxy by template matching. For the evolution
1873 analysis, they were assigned to one of four types. The
1874 only type that showed a well-defined peak in their lu-
1875 minosity distribution was Type 1 which covers the E-S_a
1876 galactic types. The characteristics of the luminosity dis-
1877 tribution were obtained by fitting a Schechter function
1878 which is

$$\phi(L)dL\phi^*(L/L^*)^\alpha e^{L/L^*} dL$$

1879 where the luminosity L^* (and its magnitude M^*) is a
1880 measure of location and α is a measure of shape.

Table 9. M_{CC}^* for SED Type 1 galaxy luminosity distribu-
tions.

z	$\Delta\mu$	$M_r^{*\alpha}$	M_B^*	M_{280}^*
0.3	0.426	-20.49	-19.06	-17.38
0.5	0.642	-20.49	-19.15	-17.84
0.7	0.822	-20.77	-19.37	-17.62
0.9	0.975	-20.54	-19.09	-17.79
1.1	1.107	-20.87	-19.23	-18.23
χ^2		3.70	2.32	12.81

^aAbsolute magnitude for the SDSS *r*-band

1881 They found that a fixed value for α works quite well
1882 for the luminosity functions of individual SED types.
1883 Examination of their estimate of M^* for Type 1 galax-
1884 ies showed that if they were converted to Curvature-
1885 cosmology magnitudes they were independent of red-
1886 shift. This is shown in Table 9 where the data are taken
1887 from the appendix to [Wolf et al. \(2003\)](#). The second
1888 column is the difference, $\Delta\mu = \mu_{CC} - \mu_{BB}$, between BB
1889 and CC, (Curvature-cosmology), distance moduli. The
1890 remaining columns show the CC absolute magnitudes
1891 for the three rest-frame bands.

1892 The last row shows the χ^2 for the five magnitudes
1893 relative to their mean using the given uncertainties (all
1894 in the range 0.14-0.23).

1895 With four degrees of freedom, the first two bands show
1896 excellent agreement with a constant value. The values
1897 for M_{280}^* have less than a 2.5% chance of being constant.
1898 However since most of the discrepancy comes from the
1899 $z = 0.3$ value of -17.38 mag and most of this band at
1900 small redshifts is outside the range of the 17 filters this
1901 discrepancy can be ignored.

1902 If this value is ignored, the χ^2 is reduced from 12.81
1903 to 6.12 (with 3 DOF) which is consistent with being con-
1904 stant. Since α is independent of redshift, the result is
1905 that if the data had been analyzed using Curvature-
1906 cosmology the magnitude for these Type 1 galaxies does
1907 not vary with redshift.

1908 Thus we have the surprising result that using Λ CDM a
1909 class of galaxies has a well-defined luminosity evolution
1910 that can be explained by Curvature-cosmology. In other
1911 words, there is no expansion.

1912 *4.8. Quasar variability in time*

1913 One of the major differences between a tired-light cos-
1914 mology and an expanding universe cosmology is that any
1915 expanding universe cosmology predicts that time varia-
1916 tions and clocks have the same dependence on redshift
1917 as does the frequency of the radiation.

1918 [Hawkins \(2010, 2003\)](#) has analyzed the variability of
1919 800 quasars covering epoch scales from 50 days to 28
1920 years. His data permitted the straightforward use of

Fourier analysis to measure the time scale of the variability. He showed that there was no significant change in the time scale of the variability with increasing redshift. He considered and rejected various explanations including that the time scales of variations were shorter in bluer pass bands or that the variations were not intrinsic but were due to intervening processes such as gravitational micro-lensing. His conclusion was either that the quasars are not at cosmological distances or that the expanding universe cosmologies are incorrect in this prediction.

Curvature-cosmology predicts the observed quasar epoch variability of zero.

4.9. The Butcher-Oemler effect

If there were evidence of significant change in the universe as a function of redshift, it would be a detrimental to any static cosmology. Probably the most important evidence for this cosmic evolution that appears to be independent of any cosmological model is the [Butcher & Oemler \(1978\)](#) effect. Although the effect has been discussed in earlier papers, the definitive paper is [Butcher & Oemler \(1984\)](#).

They observed that the fraction of blue galaxies in galactic clusters appears to increase with redshift. Clusters allow the study of large numbers of galaxies at a common distance and out to large redshifts, which makes them ideal for studies in evolution. The core regions in a cluster are dominated by early-type (elliptical and lenticular) galaxies, which have a tight correlation between their colors and magnitudes.

We can calculate R_{30} , the projected cluster-centric radius that contains 30% of the total galaxy population. The blue fraction, f_B , is defined to be the fraction of galaxies within R_{30} which are bluer than the color-magnitude relationship for that cluster.

At first sight, this may appear to be a simple test that could be done with apparent magnitudes. However to compare the ratio for distant clusters with that for nearby ones the colors must be measured in the rest frame of each cluster, hence the need to use K-corrections.

The major advantage of the Butcher-Oemler effect is that it is independent of the luminosity-distance relationship that is used. Therefore, to be more precise f_B is the fraction that has an absolute magnitude M_V , whose rest frame (B-V) color is at least 0.2 magnitudes bluer than expected. A review by [Pimblet \(2003\)](#) summarizes the important observations.

In its original form the Butcher-Oemler effect is dependent on the apparent magnitude cut-off limits. It is essential that selection effects are the same in the rest

frame for each cluster. There are further complications in that the percentage of blue galaxies may or may not depend on the richness of the cluster and the effect of contamination from background galaxies.

Although [Pimblet \(2003\)](#) concluded there was a definite effect, his Fig. 1 shows that this conclusion is open to debate. Since then there have been several attempts to measure an unambiguous effect. Even though they attempted to duplicate the original methodology of Butcher & Oemler, [Hawkins \(2003\)](#) found essentially no effect for K-selected galaxies.

[Andreon, Lobo, & Iovino \(2004\)](#) examined three clusters around $z=0.7$ and did not find clear-cut evidence for the effect. To quote one of their conclusions: *Twenty years after the original intuition by Butcher & Oemler, we are still in the process of ascertaining the reality of the Butcher-Oemler effect.*

The Butcher-Oemler effect remains uncertain, and therefore does not provide evidence to refute a static cosmology.

4.10. Fluctuations in the CMBR

In the model proposed for Curvature-cosmology these fluctuations will also occur but in this case they are due to variations in the density of the cosmic plasma. The CMBR seen through the denser gas within a galactic cluster will have lower than average temperature. [Cabr e et al. \(2006\)](#) show some support for this model in that they have correlated data from the Wilkinson Microwave Anisotropy Probe (WMAP) with galaxy samples from the SDSS DR4 galaxy survey and found a significant correlation for the intensity fluctuations with galaxy density.

4.11. Pioneer 10 acceleration.

Precise tracking of the *Pioneer 10/11*, *Galileo* and *Ulysses* spacecraft ([Anderson et al. 2002](#)) have shown an anomalous constant acceleration for *Pioneer 10* with a magnitude $(8.74 \pm 1.55) \times 10^{-10} \text{ m s}^{-2}$ directed towards the sun.

The only method for monitoring *Pioneer 10* is to measure the frequency shift of the signal returned by an active phase-locked transponder. These frequency measurements are then processed using celestial mechanics in order to get the spacecraft trajectory.

The simplicity of this acceleration and its magnitude suggests that *Pioneer 10* could be a suitable candidate for investigating the effects of Curvature-redshift. There is a major problem in that the direction of the acceleration corresponds to a blue shift whereas Curvature-redshift predicts a redshift.

Nevertheless, we will proceed, guided by the counterintuitive observation that a drag force on a satellite

actually causes it to speed up. This is because the decrease in total energy makes the satellite change orbit with a redistribution of kinetic and potential energy.

The crucial point of this analysis is that the only information available that can be used to get the *Pioneer* 10 trajectory is Doppler shift radar. There is no direct measurement of distance.

Thus the trajectory is obtained by applying celestial mechanics and requiring that the velocity matches the observed frequency shift. Since the sun produces the dominant acceleration, we can consider that all the other planetary perturbations and know drag effects have been applied to the observations and the required celestial mechanics is to be simple two-body motion.

If the observed velocity (away from the sun) is increased by an additional apparent velocity due to Curvature-redshift the orbit determination program will compensate by assuming that the spacecraft is closer to the sun than its true distance. It will be shown that this distance discrepancy produces an extra apparent acceleration that is directed towards the sun. The test of this model is whether the densities required by Curvature-redshift agree with the observed densities.

Let the actual velocity of *Pioneer* 10 at a distance r , be denoted by $v(r)$, then since the effect of Curvature-redshift is seen as an additional velocity, $\Delta v(r)$ where from Eq. 11

$$\Delta v(r) = 2\sqrt{8\pi G} \int_0^r \sqrt{\rho(r)} dr \quad (47)$$

where the factor of 2 allows for the two-way trip and the density at the distance r from the sun is $\rho(r)$. Since *Pioneer* 10 has a velocity away from the sun, this redshift shows an increase in the magnitude of its velocity.

We will assume that all the perturbations and any other accelerations that may influence the *Pioneer* 10 velocity have been removed as corrections to the observed velocity and the remaining velocity, $v(r)$, is due to the gravitational attraction of the sun. In this case the energy equation is

$$v(r)^2 = v_\infty^2 + \frac{2\mu}{r}, \quad (48)$$

where $\mu = GM$ is the gravitational constant times the mass of the sun ($\mu = 1.327 \times 10^{20} \text{ m}^3 \text{ s}^{-2}$) and v_∞ is the velocity at infinity.

The essence of this argument is that the tracking program is written to keep energy conserved so that an anomalous change in velocity, $\Delta v(r)$, will be interpreted as a change in radial distance which is

$$\Delta r = -\sqrt{\frac{2r^3}{\mu}} \Delta v(r).$$

Thus an increase in magnitude of the velocity will be treated as a decrease in radial distance which, in order to keep the total energy constant, implies an increase in the magnitude of the acceleration. Either by using Newton's gravitational equation or by differentiating Eq. 48 the acceleration $a(r)$ is given by

$$a(r) = -\frac{\mu}{r^2}. \quad (49)$$

Hence with $v_\infty = 0$ and therefore $v(r) = \sqrt{2\mu}/r$ we get

$$\Delta a(r) = \frac{2\mu}{r^3} \Delta r = \sqrt{\frac{8\mu}{r^3}} \Delta r$$

and then to the first order an increase in velocity of $\Delta v(r)$ will produce an apparent decrease in acceleration of $\Delta a(r)$, and

$$\begin{aligned} \Delta a &= 8\sqrt{\pi\mu G} r^{-3/2} \int_0^r \sqrt{\rho(r)} dr \\ &= 16\sqrt{\pi\mu G} r^{-1/2} < \sqrt{\rho(r)} > \\ &= 6.90R^{-1/2} < \sqrt{\rho(r)} > \end{aligned}$$

where for the last equations we measure the distance in AU so that $r = 1.496 \times 10^{11}R$ and the angle brackets show an average value.

Now fig. 7 from (Anderson et al. 2002) shows that after about 20 AU the anomalous acceleration is essentially constant. The first step is to get an estimate of the required density and see if is feasible.

Using the observed acceleration of $a_P = 8.74 \times 10^{-10} \text{ m s}^{-2}$ the required average density for the two-way path is $1.60 \times 10^{-20}R \text{ kg m}^{-3}$ and for $R=20$ it is $3.21 \times 10^{-19} \text{ kg m}^{-3}$.

The only constituent of the interplanetary medium that approaches this density is dust. One estimate by Le Sergeant D'Hendecourt & Lamy (1980) of the interplanetary dust density at 1 AU is $1.3 \times 10^{-19} \text{ kg m}^{-3}$ and more recently, Grun et al. (1999) suggests a value of $10^{-19} \text{ kg m}^{-3}$ which is consistent with their earlier estimate of $9.6 \times 10^{-20} \text{ kg m}^{-3}$ (Grun, Zook, Fechtig, & Giese 1985).

Although the authors do not provide uncertainties, it is clear that their densities could be in error by a factor of two or more. The main difficulties are the paucity of information and that the observations do not span the complete range of grain sizes.

The meteoroid experiment on board *Pioneer* 10 measures the flux of grains with masses larger than 10^{-10} g . The results show that after it left the influence of Jupiter the flux (Anderson et al. 2002) was essentially constant (in fact there may be a slight rise) out to a distance of 18 AU.

It is thought that most of the grains are being continuously produced in the Kuiper belt. As the dust orbits evolve inwards due to Poynting-Robertson drag and planetary perturbations, they achieve a roughly constant spatial density. The conclusion is that interplanetary dust could provide the required density to explain the anomalous acceleration by a frequency shift due to Curvature-redshift.

Overall, this analysis has shown that it is possible to explain the acceleration anomaly of *Pioneer* 10 but that a more definitive result requires Curvature-redshift to be included in the fitting program and more accurate estimates of the dust density are certainly needed. Subject to the caveat about the dust density, Curvature-redshift could explain the anomaly in the acceleration of *Pioneer* 10 (and by inference other spacecraft).

Not only can Curvature-cosmology explain the anomalous Pioneer 10 acceleration, it has a feasible prediction of its value.

4.12. *The Sunyaev-Zel'dovich effect*

The Sunyaev-Zel'dovich effect (Sunyaev & Zeldovich 1970; Peebles 1993) is the effect of Thompson scattering of background radiation by free electrons in the intervening medium. The technique depends on knowing the spectrum of the background source and then measuring the changes in the spectrum due to the intervening plasma.

In particular, it is the scattering in both angle and frequency of the cosmic microwave background radiation (CMBR) by electrons in the cosmic plasma. Because of the rapidly changing density (like $(1+z)^3$) with redshift this is an important effect in Λ CDM cosmology. The effect is often characterized by the dimensionless Compton y -parameter, which for a distance x through non-relativistic thermal plasma with an electron density of N_e has the value

$$y = \frac{kT_e}{m_e c^2} \sigma_T N_e x = 3.46 \times 10^{-16} N_e T_e x \text{ Mpc}, \quad (50)$$

where σ_T is the Thompson cross-section. An object at redshift z is at the distance $x = R_\chi = 5.80 \times 10^3 N_e^{1/2} \log(1+z)$ Mpc. Hence, using $T_e = 2.62 \times 10^9$ K, $N_e = 1.35 \text{ m}^{-3}$ we get $y = 9.2 \times 10^{-6} \log(1+z)$.

Using the CMBR as a source the Sunyaev-Zel'dovich effect has been observed and Mather et al. (1990) report an observed upper limit of $y = 0.001$, and more recently Fixsen et al. (1996) report $y = 1.5 \times 10^{-5}$.

Using this limit with Eq. 50 shows that there is no effect in Curvature-cosmology if $z < 4.1$. Although in Curvature-cosmology the CMBR has a more local origin it is of interest to note that this analysis assumes that each photon has many Compton interactions.

For this electron density, the Compton mean free path is 575 Gpc whereas the distance to $z = 4.1$ is about 3.7 Gpc which means that a negligible number of the photons will have an interaction with the high temperature electrons.

Furthermore the photon energy distribution for a single interaction has a different spectrum for that for the normal Sunyaev-Zel'dovich effect

(Longair 1991; Sunyaev & Zeldovich 1980). Bielby & Shanks (2007) extend the results of Lieu, Mittaz, & Zhang (2006) to show that not only was the Sunyaev-Zel'dovich effect less than what was expected but that it tended to disappear as the redshift went from 0.1 to 0.3. The conclusion is that Curvature-cosmology is completely consistent with the experimental observations of the Sunyaev-Zel'dovich effect on the CMBR. Thus the Sunyaev-Zel'dovich effect is important in standard cosmology it is not important in Curvature-cosmology.

4.13. *Gravitational lensing.*

There are many gravitational lens where a quasar or distant galaxy has one or more images produced by a nearer lensing galaxy or cluster of galaxies. A set of these lensing systems has been examined in the context of Curvature-cosmology to see if it offers a consistent and possibly simpler explanation. The two important measures are the prediction of the mass of the lensing galaxy and the determination of the Hubble constant from the time delays between variations in the luminosity of different images. Since the delay measurement is easily done, all that is needed is to measure the different path lengths. This path difference involves both geometric and general relativistic corrections.

One of the remarkable properties of gravitational lenses is that the geometry is completely determined by a two-dimensional lensing potential which can be expressed in terms of a surface density at the position of the lensing galaxy. For thin lenses, any two systems with the same surface density distribution have the same lens effect. Now the usual way to determine the surface density is to measure the widths of spectral lines, assume that the width is due to velocity and then use the virial theorem to obtain the surface density.

However in Curvature-cosmology the widths of spectral lines are likely to have a large component due to the effects of Curvature-redshift from dust and gas in the lensing object. Thus the widths are not a reliable measure of area density and this method cannot be used.

4.14. *Lyman-alpha forest*

The Lyman- α ($\text{Ly}\alpha$) forest is the large number of absorption lines seen in the spectra of quasars. Most

of the lines are due to absorption by clouds of neutral hydrogen in the line of sight to the quasar. Some of the lines are due to other elements or due to Lyman- β absorption.

Because of the redshift between the absorbing cloud and us, the lines are spread out over a range of wavelengths. Usually the analysis is confined to lines between the Ly α (at a wavelength of 121.6 nm) and Ly β (at 102.5 nm). Thus, each quasar provides a relatively narrow spectrum of Ly- α lines at a redshift just less than that for the quasar. Since the advent of spacecraft telescopes, in which can observe the ultraviolet lines, and by using many quasars the complete redshift range up to the most distant quasar has been covered. The large redshift range makes the Lyman α spectra potentially a powerful cosmological tool.

The obvious cosmological observation is the density of lines as a function of redshift but as discussed by Rauch (1998) in an excellent review, there are many important observational problems.

The first, which has now been overcome, is that the spectra must have sufficient resolution to resolve every line. The second is that most lines are very weak and the number of resolved lines can depend greatly on the signal-to-noise ratio. This is accentuated because the steep spectrum for the density of lines as a function of their strength means that a small decrease in the acceptance level can drastically increase the number of observed lines. The third problem is that each quasar only provides a set of lines in a narrow range of redshift and there are considerable difficulties in getting uniform cross-calibrations.

In addition to these problems, it will be shown that Curvature-redshift can have a profound effect on the interpretation of the line widths and column densities.

Since in Curvature-cosmology, the distribution of clouds is independent of time or distance the expected density of lines as a function of redshift is

$$\frac{dn}{dz} = \frac{AcN_\epsilon}{H(1+z)}, \quad (51)$$

where N_0 is the volume density and A is the average area of a cloud. Most observers have fitted a power law with the form $(1+z)^\gamma$ to the observed line densities with a wide range of results. They vary from $\gamma = 1.89$ to $\gamma = 5.5$ (Rauch 1998). All of which are inconsistent with the Curvature-cosmology prediction of $\gamma = -1$.

In Curvature-cosmology, there is the additional effect that much of the line broadening may be due to Curvature-redshift. Curvature-redshift will be operating within the clouds so that the observed line width will be a combination of the usual Voigt profile and the

change in the effective central frequency as the photons pass through the cloud. If the cloud has a density $\rho(x)$ at the point x , measured along the photon trajectory then the change in frequency from the entering frequency due to Curvature-redshift is

$$\frac{\Delta\nu}{\nu} = \frac{1}{c} \int \sqrt{8\pi G\rho(x)} dx.$$

In units of $N(x) = \rho(x)/m_H$ this is (with N in m^{-3} and dx in kpc)

$$\frac{\Delta\nu}{\nu} = -\frac{\Delta\lambda}{\lambda} = \int 1.724 \times 10^{-7} \sqrt{N(x)} dx.$$

Then the final profile will be the combination of the natural line width, the Doppler width due to temperature, any width due to bulk motions and the Curvature-redshift width. Now assuming pure hydrogen, the hydrogen column density is given by $N_H = \int N(x) dx$.

Although it is unlikely that the line of sight goes through the center of the cloud, it is reasonable to expect a roughly symmetric distribution of gas with a shape similar to a Gaussian. We can define an effective density width by

$$x_w^2 = \int (x - \bar{x})^2 N(x) dx / \int N(x) dx.$$

Also define $N_0 = N_H/x_w$ and an effective velocity width $\Delta v = 51.68\eta x_w \sqrt{N_0}$ and where η is a small numeric constant that depends on the exact shape of the density distribution. Eliminating the central density, we get (with x_w in kpc)

$$\Delta v^2 = 8.656 \times 10^{-17} \eta^2 N_H x_w. \quad (52)$$

For values $N_H = 10^{19} \text{ m}^{-2}$, $x_w = 1 \text{ kpc}$ and with $\eta = 1$ we get $\Delta v = 29 \text{ km s}^{-1}$.

Since there is a wide variation in column densities and the effective widths are poorly known, it is clear that Curvature-redshift could completely dominate many of the Lyman- α line widths and the others would require a convolution of the Doppler profile with the Curvature-redshift density effect. What is also apparent is that the very broad absorption lines may be due to Curvature-redshift acting in very dense clouds.

Although there is uncertainty about the observed relationship between the line width and the column density, we note that for a fixed effective density width, Eq. 52 predicts a square relationship that may be compared with the exponent of 2.1 ± 0.3 found by Petini et al. (1990). Clearly, there needs to be a complete re-evaluation of profile shapes, column densities, and cloud statistics that allows for the effects of Curvature-cosmology. We must await this analysis to see whether the Lyman- α forest can provide a critical test of Curvature-cosmology.

4.15. Nuclear abundances

One of the successes of Λ CDM cosmology is in its explanation of the primordial abundances of the light elements. Since the proposed Curvature-cosmology is static, there must be another method of getting the ‘primordial’ abundances of light elements. In Curvature-cosmology, the primordial abundance refers to the abundance in the cosmic gas from which the galaxies are formed.

The first point to note is that in Curvature-cosmology the predicted temperature of the cosmic plasma is 2.465×10^9 K at which temperature nuclear reactions can proceed.

It is postulated that in Curvature-cosmology there is a continuous recycling of material from the cosmic plasma to galaxies and stars and then back to the gas. Because of the high temperature, nuclear reactions will take place whereby the more complex nuclei are broken down to hydrogen.

4.16. Galactic rotation curves

One of the most puzzling questions in astronomy is: why does the observed velocity of rotation in spiral galaxies not go to zero towards the edge of the galaxy. Simple Keplerian mechanics suggest that there should be a rapid rise to a maximum and then a decrease in velocity that is inversely proportional to the square root of the radius once nearly all the mass has been passed.

Although the details vary between galaxies, the observations typically show a rapid rise and then an essentially constant tangential velocity as a function of radius out to distances where the velocity cannot be measured due to lack of material. The Λ CDM explanation is that this is due to the gravitational attraction of a halo of dark matter that extends well beyond the galaxy. We examine whether this rotation curve can be explained by Curvature-redshift.

Observations show that our own Galaxy and other spiral galaxies have a gas halo that is larger than the main concentration of stars. It is clear that if the observed redshifts are due to Curvature-redshift acting within this halo, the halo must be asymmetric; otherwise, it could not produce the asymmetric rotation curve.

Now the observed velocities in the flat part of the curves are typically 100 to 200 km s^{-1} . The first step is to see if Curvature-redshift provides the right magnitude for the velocity. For a gas with an average density of N_H the predicted redshift (in velocity units) is $5.17 \times 10^{-2} d \sqrt{N} \text{ km s}^{-1}$ where d is the distance in kpc. For realistic values of $d = 10$ kpc and $N = 1.0 \times 10^5 \text{ m}^{-3}$ the velocity is 163 km s^{-1} . Thus, the magnitude is feasible.

Although there could be a natural asymmetry in a particular galaxy, the fact that the flattened rotation curve is seen for most spiral galaxies suggests that there is a common cause for the asymmetry.

A partial explanation is that the halos are rotating more like a solid object and that the observed rotation is genuine.

Another possibility is that the asymmetry could arise from ram pressure. Since most galaxies are moving relative to the cosmic medium, it is expected that there will be an enhanced density towards the leading point of the galaxy. This asymmetric density could produce an apparent velocity gradient across the galaxy that could explain the apparent rotation curve.

Naturally, there would be range of orientations and the apparent velocity gradient must be added to any intrinsic rotation curve to produce a wide diversity of results. Thus, Curvature-redshift could explain the galactic rotation curves if there is an asymmetric distribution of material in the galactic halo.

Both cosmologies have problems with galactic rotation curves. Λ CDM cosmology not only requires dark matter but does not have any definite models for its distribution. Curvature-cosmology has the problem of achieving sufficient asymmetry to mimic a rotation curve.

4.17. Redshifts in our Galaxy

In our Galaxy, the Milky Way, there is an interesting prediction. The density of the interstellar ionized gas is high enough to inhibit Curvature-redshift for radio frequencies.

From Eq. 36 it was shown that for wavelengths longer than about $20.6 N_e^{-1/2} \text{ m}$ the effect of refractive index in fully ionized plasma will inhibit Curvature-redshift. The refractive index of neutral hydrogen is too low to inhibit Curvature-redshift. However, any fully ionized plasma with $N_e > 10^4 \text{ m}^{-3}$ will inhibit Curvature-redshift for the 21 cm hydrogen line. Since the local interstellar medium has an electron density of about 10^5 m^{-3} Curvature-redshift will be inhibited for the 21 cm hydrogen in these local regions.

Thus for sight lines close to the Galactic plane we can assume a similar density and thus a similar inhibition with the result that the observed radio redshifts can be correctly interpreted as genuine velocities. Thus, there is little change needed to the current picture of galactic structure and rotation derived from 21 cm redshifts. However, there may be some Curvature-redshift present in sight lines away from the plane and especially in the Galactic halo.

Since optical redshifts have the full effects of Curvature-redshift, it should be possible to find objects

with discrepant redshifts where the optical redshift is greater than the radio redshift. The difficulty is that the two types of radiation are produced in radically different environments: the optical in compact high temperature objects, such as stars, and the radio in very low-density cold clouds. In addition, there is the complication that within the galactic plane, optical extinction due to dust limits the optical range to about 1 kpc.

Curvature-redshift may help to explain an old stellar mystery. There is a long history provided by [Arp \(1992\)](#) of observations of anomalous redshifts in bright hot stars, which is called the K-term or K-effect.

[Allen \(1976\)](#) states that B₀ stars typically show an excess redshift of 5.1 m s⁻¹, A₀ have 1.4 km s⁻¹ and F₀ have 0.3 km s⁻¹. This can be explained if these stars have a large corona that produces a Curvature-redshift.

It is probably no coincidence that such stars have large stellar winds and mass outflows. In order to see if it is feasible let us consider a simple model for the outflow in which the material has a constant velocity v_0 , and conservation of matter (Gauss's Law) then requires that the density has inverse square law dependence. Although this is incorrect at small stellar radii, it is a reasonable approximation further from the star.

Then if ρ_1 is the density at some inner radius r_1 , then integration of Eq. 25 out to a radius r_2 , the expected redshift in velocity units is

$$v = \sqrt{\frac{2GM}{v_o}} \log\left(\frac{r_2}{r_1}\right),$$

where \dot{M} is the observed stellar mass-loss-rate. Then with \dot{M} in solar masses per year, with v and v_0 in km s⁻¹, the redshift is

$$v = 91.7 \sqrt{\frac{\dot{M}}{v_o}} \log\left(\frac{r_2}{r_1}\right) \text{ km s}^{-1},$$

With $\dot{M} = 10^{-5} M_\odot \text{ yr}^{-1}$ [Cassinelli \(1979\)](#), $v_0 = 1 \text{ km s}^{-1}$ and $r_2/r_1 = 10^3$ the predicted redshift (in velocity units) is 2 km s⁻¹ which is in reasonable agreement with the observed K-effects mentioned above.

4.18. Anomalous redshifts

[Arp \(1987\)](#); [Ratcliffe \(2010\)](#) have argued that there is strong observational evidence for anomalous redshifts between quasars and galaxies.

Typically if there is a quasar very close to a galaxy with a material bridge or other evidence that suggests that they are associated. [Chu et al. \(1998\)](#) report on five X-ray emitting blue stellar objects located less than 12 arcmin from the X-ray Seyfert galaxy NGC 3516. In this case the association is that the objects lie close

to a straight line on either side of the galaxy and that their redshifts are proportional to $\log(\theta)$ where θ is the angular distance from the central galaxy.

Furthermore the line of objects is within a few degrees of the minor axis of NGC 3516. The measured redshifts are 0.33, 0.69, 0.93, 1.4 and 2.1. NGC 3516 is a barred spiral galaxy and it has a redshift of 0.00884.

Can Curvature-cosmology explain this redshift anomaly? If the objects are seen through a large dense cloud, such as a galactic halo, then Curvature-redshift will produce an extra redshift due to the photons passage through the cloud. the extra redshift, δ , is

$$\delta = 1.72 \times 10^{-10} \int \sqrt{N(x)} dx,$$

where $N(x)$ is the number density and distances are measured in pc. If z is the cosmological redshift then the extra-observed redshift is $\Delta z = (1 + z)(e^\delta - 1)$.

In order to achieve an extra redshift $\delta \approx 1$ with a distance of 10⁴ pc the gas number density must be about 3 × 10¹¹ m⁻³. Now although cold interstellar molecular clouds can have densities reaching this value it is still a very high density.

But if the size is increased by a factor of two, the required density is decreased by a factor of four. Moreover the objects with the largest redshifts are the furthest away from the galaxy. These redshifts could be explained by Curvature-redshift in a very large, very dense galactic halo with a hole in the middle.

Since NGC 3516 has a very low redshift and is seen nearly face on, the implication is that this gas cloud is probably shaped like a torus and it lies in the galactic plane of NGC3516. A further test is to compare an estimate of the mass of this torus with that for a typical galaxy. Since a torus formed by the rotation of a circle with radius r about a axis in the plane of the circle where the radius of rotation is R , its volume is $V = 2\pi^2 Rr^2$. With R and r in kpc and an average density of N its mass is $M = 0.484 Rr^2 N M_{sun}$. Then with $R = 15$ kpc, $r = 10$ kpc and $N = 3 \times 10^{11}$ the mass is $2 \times 10^{14} M_{sun}$ which considerably larger than a normal galaxy.

Since these anomalous redshifts are completely outside any standard cosmological model, the only reason that these observations are not fatal to standard cosmological is their controversial nature.

4.19. Voids

If Curvature-cosmology is valid then the redshift of the galaxies in the Coma cluster (Section 4.5) will have been increased, on average, by the additional redshift due to the intergalactic gas. Thus, they will have, on average, a larger redshift than an isolated galaxy at the same distance.

Table 10. Velocity at, and average velocity within various projected radii in the Coma cluster (distance = 87.1 Mpc).

Radius ^a /Mpc	Velocity /km s ⁻¹	Mean velocity /km s ⁻¹
0.0	2327.7	2327.7
0.5	1477.7	1764.8
1.0	1033.4	1342.5
1.5	803.3	1096.9
2.0	658.6	933.2
2.5	557.0	814.4
3.0	481.0	723.3
3.5	421.7	650.7
4.0	374.0	541.2
4.5	334.8	541.2
5.0	302.0	498.7

^a projected radius

Table 10 shows the predicted (effective) velocity for a galaxy in the center plane of the Coma cluster as a function of the projected radius. The second column is the velocity at that exact radius and the third column shows the average velocity of galaxies (uniformly spread in area) within that radius. This simulation also showed that the average velocity offset for the galaxies in the Coma cluster is 1206 km s⁻¹ which means that the redshift of the center of the Coma cluster is 6926-1206=5720 km s⁻¹. This offset is important for calculating the Hubble constant which from these figures is 5270/87.1=65.7 km s⁻¹ Mpc⁻¹.

In addition, the redshift of objects seen through a cluster will be increased by Curvature-redshift from the intergalactic gas.

Karoji, Nottale, & Vigier (1976) claim to have seen this effect. They examined radio galaxies and classified them into region A if their light does not pass through a cluster and region B if their light passes through a cluster. They found no significant differences in magnitudes between the two regions but they did find a significant difference in the average redshift that was consistent over the complete range.

Their result is that radio galaxies seen through a cluster had an average extra redshift (in velocity units) of 2412±1327 km s⁻¹. Overall the difference in the distance modulus was $\mu = 0.16 \pm 0.04$, which is just significant.

Since the density and distribution of the gas in the clusters is unknown and the limiting radius of the cluster is not stated, it is impossible to get an accurate prediction.

Nevertheless, we note that for the Coma cluster with a radius of 2 Mpc the average extra redshift (from Table 10 with a factor of two) corresponds to 1866 km s⁻¹ showing that Curvature-cosmology could explain the effect.

In a different study, Nottale (1976) and Nottale & Vigier (1977) compared the magnitude of the brightest galaxy in a cluster with that in another cluster with similar redshift. They found that there was no significant difference in magnitudes between clusters but that the clusters with the largest number of galaxies had the higher redshift difference between the pairs.

On average the redshift difference (in velocity units) was 292±85 km s⁻¹. This can be explained by the expected correlation between the number of galaxies and size and density of the intergalactic gas. However it should be noted that these observations have been disputed by Rood & Struble (1982).

In his review of voids in the distribution of galaxies, Rood (1988) quotes Mayall (1960) who observed a large void in the distribution of galaxies in front of the Coma cluster. This void has a magnitude of about 3000 km s⁻¹, which although somewhat larger, is not inconsistent with the expected value of about 1200 km s⁻¹.

In other words, the Coma cluster galaxies have an extra Curvature-redshift due to the intergalactic gas. However, the galaxies just outside the cluster nearer to us do not have this extra redshift and would appear to be closer to us. Hence, we see an apparent void in the redshift distribution in front of the Coma cluster.

A consequence of gas clouds and Curvature-redshift is that the distribution of redshifts is similar to but not identical to the distribution of z distances. Galaxies that are behind a cloud will have a higher redshift than would be expected from a simple redshift distance relationship.

Thus, we would expect to see anomalous voids and enhancements in the redshift distribution. This will be accentuated if the gas clouds have a higher than average density of galaxies.

de Lapparent et al. (1986) show a redshift plot for a region of the sky that includes the Coma cluster. Their data are from the Center for Astrophysics redshift survey and their plot clearly shows several voids. They suggest that the galaxies are distributed on the surfaces of shells. However, this distribution could also arise from the effects of Curvature-redshift in clouds of gas.

4.20. Entropy

Consider a stellar cluster or an isolated cloud of gas in which collisions are negligible or elastic. In either case the virial theorem states that the average kinetic energy K , is related to the average potential energy V ,

2576 by the equation $V = V_0 - 2K$ where V_0 is the poten-
 2577 tial energy when there is zero kinetic energy. Let U be
 2578 the total energy then $U = K + V = V_0 - K$. Thus,
 2579 we get the somewhat paradoxical situation that since
 2580 V_0 is constant; an increase in total energy can cause a
 2581 decrease in kinetic energy. This happens because the av-
 2582 erage potential energy has increased by approximately
 2583 twice as much as the loss in kinetic energy. Since the
 2584 temperature is proportional to (or at the least a mono-
 2585 tonic increasing function of) the average kinetic energy,
 2586 it is apparent that an increase in total energy leads to a
 2587 decrease in temperature. This explains the often-quoted
 2588 remark that a self-gravitationally bound gas cloud has
 2589 a negative specific heat capacity. Thus, when gravity
 2590 is involved the whole construct of thermodynamics and
 2591 entropy needs to be reconsidered.

2592 One of the common statements of the second law of
 2593 thermodynamics is that (Longair 1991): *The energy of*
 2594 *the universe is Constant: the entropy of the Universe*
 2595 *tends to a maximum,* (Feynman 1965): *the entropy of*
 2596 *the universe is always increasing* or from Wikipedia *the*
 2597 *second law of thermodynamics is an expression of the*
 2598 *universal law of increasing entropy, stating that the en-*
 2599 *tropy of an isolated system which is not in equilibrium*
 2600 *will tend to increase over time, approaching a maximum*
 2601 *value at equilibrium.*

2602 Now the normal proof of the second law considers the
 2603 operation of reversible and non-reversible heat engines
 2604 working between two or more heat reservoirs. If we use a
 2605 self-gravitating gas cloud as a heat reservoir then we will
 2606 get quite different results since the extraction of energy
 2607 from it will lead to an increase in its temperature. Thus
 2608 if the universe is dominated by gravity the second law
 2609 of thermodynamics needs reconsideration. In addition,
 2610 it should be noted that we cannot have a shield that
 2611 hides gravity. To put it another way there is no adia-
 2612 batic container that is beyond the influence of external
 2613 gravitational fields. Thus we cannot have an isolated
 2614 system.

2615 This discussion shows that in a static finite universe
 2616 dominated by gravity simple discussions of the second
 2617 law of thermodynamics can be misleading. The presence
 2618 of gravity means that it is impossible to have an isolated
 2619 system. To be convincing any proof of the second law
 2620 of thermodynamics should include the universe and its
 2621 gravitational interactions in the proof.

2622 4.21. Olber's Paradox

2623 For Curvature-cosmology, Olber's Paradox is not a
 2624 problem. Curvature-redshift is sufficient to move dis-
 2625 tant starlight out of the visible band. Visible light from
 2626 distant galaxies is shifted into the infrared where it is no

2627 longer seen. Of course, with a finite universe, there is the
 2628 problem of conservation of energy and why we are not
 2629 saturated with very low frequency radiation produced by
 2630 Curvature-redshift. These low-energy photons are even-
 2631 tually absorbed by the cosmic plasma. Everything is re-
 2632 cycled. The plasma radiates energy into the microwave
 2633 background radiation and into X-rays. The galaxies de-
 2634 velop from the cosmic plasma and pass through their
 2635 normal evolution. Eventually all their material is re-
 2636 turned to the cosmic plasma. Note that very little, if
 2637 any, is locked up into black holes. Curvature-pressure
 2638 causes most of the material from highly compact objects
 2639 to be returned to the surrounding region as jets.

2640 4.22. Philip's relation

2641 Phillips (1993) Showed that there was a good corre-
 2642 lation between the peak magnitude and the width of
 2643 the light curve for Type Ia supernova. For the Philip's
 2644 relation to be meaningful, it must be between the abso-
 2645 lute magnitude and the width corrected for its $(1 + z)$
 2646 dependence.

2647 The slope of the regression of the absolute magni-
 2648 tudes (using the Λ CDM model and the intrinsic anal-
 2649 ysis) of Type Ia supernova for all the supernova versus
 2650 the widths divided by $(1 + z)$ is (-0.009 ± 0.091) . Which
 2651 shows that for these observations of Type I a supernova
 2652 there is no significant Phillip's relation which implies
 2653 that SALT2 estimates of this relation may be an arti-
 2654 fact of the SALT2 analysis.

2655 5. CONCLUSIONS

2656 This is a brief summary of the quantitative obser-
 2657 vations that are relevant to the Curvature-cosmology
 2658 model. The predicted Hubble's constant is

$$2659 H_0 = c/R \text{ s}^{-1} \tag{53}$$

$$2660 = 2.364 \times 10^{-5} \sqrt{\rho} \text{ s}^{-1}$$

$$2661 = 9.6352 \times 10^{-19} \sqrt{N_\epsilon} \text{ s}^{-1} \tag{54}$$

$$2662 = 29.73 \sqrt{N_\epsilon} \text{ kms}^{-1} \text{ Mpc}^{-1}$$

$$2663 = 41.30 \text{ kms}^{-1} \text{ Mpc}^{-1},$$

2664 where the last line has used $N_\epsilon = 1.93$ from section 4.2.
 2665 This value is significantly less than the current value of
 $H_0 \approx 0.70$. However these measurements were based
 2666 the standard model. A valid test would be s to measure
 2667 the distances and redshifts using Curvature-cosmology.

For the 1,652 Type Ia supernova analyzed in Part A
 the light curve width is

$$w_{obs}(z) = 1.060 \pm 0.009 + (1.080 \pm 0.042) z.$$

and the regression of the absolute magnitudes as a function of redshift is

$$M(z) = -17.582 \pm 0.012 + (0.030 \pm 0.057) z,$$

Both results shows very strong support for Curvature-cosmology

It has been shown that the X-ray data in the range from about 10 Kev to about 300 kev can be explained by bremsstrahlung from the cosmic gas. The fitted temperature was $2.62 \pm 0.13 \times 10^9$ K, whereas the predicted temperature is $2.46 \pm 0.04 \times 10^9$ K, which shows excellent agreement. The fitted density for the cosmic plasma is $N_e = 1.93 \pm 0.04$ hydrogen atoms per m^3 .

For CMBR Curvature-cosmology predicts a temperature of 2.736 which is comparable with the observed temperature of 2.72548 ± 0.00057 K.

The standard cosmology predicts that the distribution of surface brightness should have an exponent of four, whereas Curvature-cosmology predicts an exponent of one. The result is $n = 1.38 \pm 0.13$ which is in agreement with unity.

Curvature-cosmology does not need dark matter to explain the velocity dispersion in clusters of galaxies or the shape of galactic rotation curves. Nor does it need dark energy to explain type 1a supernova observations.

For angular size the conclusion is in favor of Curvature-cosmology.

An analysis of many galaxies that have multiple observed bands show no evidence of evolution.

Curvature-cosmology predicts the observed quasar epoch variability of zero.

The Butcher-Oemler effect remains uncertain, and therefore does not provide evidence to refute a static cosmology.

Fluctuations in the CMBR can be explained a density fluctuations in the cosmic plasma.

Not only can Curvature-cosmology explain the anomalous Pioneer 10 acceleration, it has a feasible prediction of its value.

6. AUTHOR BIOGRAPHY

David F. Crawford was born at Griffith, NSW, Australia in 1937. He graduated BSc and PhD from School of Physics, University of Sydney. Half of his PhD thesis was on designing and building a Geiger counter array to study cosmic ray air-showers and the second half on programming a three-dimensional Monte Carlo simulation on the computer Silliac to calculate the energy and structure of electron-photon cascades. The results published in a 1,512-page book "Electron-photon Shower Distribution Function" by H. Messel and D.F. Crawford, Pergamon Press, 1970.

He worked for two years from 1966 at Cornell University learning radar Astronomy. From 1969 to his retirement in 2003, He provided computer analysis of observations from the Molonglo Radio Telescope. He is a member of the Australian Astronomical Society. He has been an author in 33 papers published in refereed journals. Since he wrote his first program in 1959, He has had a major interest in computers and programming especially in the use of computers to analyze observations and apply them to astrophysical theories. He also have a long-time interest in the foundations of cosmology.

ACKNOWLEDGMENTS

This research has made use of the NASA/IPAC Extragalactic Database (NED) that is operated by the Jet Propulsion Laboratory, California Institute of Technology, under contract with the National Aeronautics and Space Administration. The calculations have used Ubuntu Linux and the graphics have used the DISLIN plotting library provided by the Max-Planck-Institute in Lindau.

REFERENCES

- Allen, C. W. 1976, *Astrophysical Quantities*
- Amanullah, R., Lidman, C., Rubin, D., et al. 2010, *The Astrophysical Journal*, 716, 712, doi: [10.1088/0004-637X/716/1/712](https://doi.org/10.1088/0004-637X/716/1/712)
- Anderson, J. D., Laing, P. A., Lau, E. L., et al. 2002, *PhRvD*, 65, 082004, doi: [10.1103/PhysRevD.65.082004](https://doi.org/10.1103/PhysRevD.65.082004)
- Andreon, S., Lobo, C., & Iovino, A. 2004, *MNRAS*, 349, 889, doi: [10.1111/j.1365-2966.2004.07554.x](https://doi.org/10.1111/j.1365-2966.2004.07554.x)
- Arp, H. 1987, *Quasars, redshifts, and controversies*
- . 1992, *Monthly Notices of the Royal Astronomical Society*, 258, 800, doi: [10.1093/mnras/258.4.800](https://doi.org/10.1093/mnras/258.4.800)
- Beijersbergen, M. 2003, PhD thesis, University of Groningen, Netherlands
- Betoule, M., Kessler, R., Guy, J., et al. 2014, *Astronomy and Astrophysics*, 568, A22, doi: [10.1051/0004-6361/201423413](https://doi.org/10.1051/0004-6361/201423413)

- 2751 Bielby, R. M., & Shanks, T. 2007, *Monthly Notices of the*
 2752 *Royal Astronomical Society*, 382, 1196,
 2753 doi: [10.1111/j.1365-2966.2007.12456.x](https://doi.org/10.1111/j.1365-2966.2007.12456.x)
- 2754 Blanton, M. R., & Moustakas, J. 2009, *Annual Review of*
 2755 *Astronomy and Astrophysics*, 47, 159,
 2756 doi: [10.1146/annurev-astro-082708-101734](https://doi.org/10.1146/annurev-astro-082708-101734)
- 2757 Blondin, S., Davis, T. M., Krisciunas, K., et al. 2008, *The*
 2758 *Astrophysical Journal*, 682, 724, doi: [10.1086/589568](https://doi.org/10.1086/589568)
- 2759 Born, M., & Wolf, E. 1999, *Principles of Optics*
 2760 Braginskij, V. B., & Panov, V. I. 1971, *Uspekhi*
 2761 *Fizicheskikh Nauk*, 105, 779
- 2762 Briel, U. G., Henry, J. P., & Boehringer, H. 1992, *A&A*,
 2763 259, L31
- 2764 Buchalter, A., Helfand, D. J., Becker, R. H., & White,
 2765 R. L. 1998, *The Astrophysical Journal*, 494, 503,
 2766 doi: [10.1086/305236](https://doi.org/10.1086/305236)
- 2767 Butcher, H., & Oemler, A., J. 1978, *The Astrophysical*
 2768 *Journal*, 219, 18, doi: [10.1086/155751](https://doi.org/10.1086/155751)
- 2769 —. 1984, *The Astrophysical Journal*, 285, 426,
 2770 doi: [10.1086/162519](https://doi.org/10.1086/162519)
- 2771 Cabré, A., Gaztañaga, E., Manera, M., Fosalba, P., &
 2772 Castander, F. 2006, *Monthly Notices of the Royal*
 2773 *Astronomical Society*, 372, L23,
 2774 doi: [10.1111/j.1745-3933.2006.00218.x](https://doi.org/10.1111/j.1745-3933.2006.00218.x)
- 2775 Carlip, S. 1998, *American Journal of Physics*, 66, 409,
 2776 doi: [10.1119/1.18885](https://doi.org/10.1119/1.18885)
- 2777 Cassinelli, J. P. 1979, *Annual Review of Astronomy and*
 2778 *Astrophysics*, 17, 275,
 2779 doi: [10.1146/annurev.aa.17.090179.001423](https://doi.org/10.1146/annurev.aa.17.090179.001423)
- 2780 Chu, Y., Wei, J., Hu, J., Zhu, X., & Arp, H. 1998, *The*
 2781 *Astrophysical Journal*, 500, 596, doi: [10.1086/305779](https://doi.org/10.1086/305779)
- 2782 Colless, M., & Dunn, A. M. 1996, *ApJ*, 458, 435,
 2783 doi: [10.1086/176827](https://doi.org/10.1086/176827)
- 2784 Conley, A., Guy, J., Sullivan, M., et al. 2011, *The*
 2785 *Astrophysics Journal Supplement Series*, 192, 1,
 2786 doi: [10.1088/0067-0049/192/1/1](https://doi.org/10.1088/0067-0049/192/1/1)
- 2787 Cowsik, R., & Kobetich, E. J. 1972, *The Astrophysical*
 2788 *Journal*, 177, 585, doi: [10.1086/151735](https://doi.org/10.1086/151735)
- 2789 Crawford, D. F. 1987a, *Australian Journal of Physics*, 40,
 2790 459, doi: [10.1071/PH870459](https://doi.org/10.1071/PH870459)
- 2791 —. 1987b, *Australian Journal of Physics*, 40, 449,
 2792 doi: [10.1071/PH870449](https://doi.org/10.1071/PH870449)
- 2793 —. 1991, *ApJ*, 377, 1, doi: [10.1086/170330](https://doi.org/10.1086/170330)
- 2794 —. 1993, *ApJ*, 410, 488, doi: [10.1086/172765](https://doi.org/10.1086/172765)
- 2795 —. 1995a, *ApJ*, 440, 466, doi: [10.1086/175288](https://doi.org/10.1086/175288)
- 2796 —. 1995b, *ApJ*, 441, 488, doi: [10.1086/175375](https://doi.org/10.1086/175375)
- 2797 —. 1998, arXiv e-prints, astro.
 2798 <https://arxiv.org/abs/astro-ph/9803009>
- 2799 —. 1999a, *Australian Journal of Physics*, 52, 753,
 2800 doi: [10.1071/PH98065](https://doi.org/10.1071/PH98065)
- 2801 —. 1999b, arXiv e-prints, astro.
 2802 <https://arxiv.org/abs/astro-ph/9904150>
- 2803 —. 2006, *Curvature Cosmology*
- 2804 —. 2009a, arXiv e-prints, arXiv:0901.4169.
 2805 <https://arxiv.org/abs/0901.4169>
- 2806 —. 2009b, arXiv e-prints, arXiv:0901.4172.
 2807 <https://arxiv.org/abs/0901.4172>
- 2808 —. 2022, In Press, 0, 09, doi =
 2809 10.1142/S0218271819500822, adsnote = Provided by the
 2810 SAO/NASA Astrophysics Data System
- 2811 de Lapparent, V., Geller, M. J., & Huchra, J. P. 1986,
 2812 *ApJL*, 302, L1, doi: [10.1086/184625](https://doi.org/10.1086/184625)
- 2813 Dennis, B. R., Suri, A. N., & Frost, K. J. 1973, *The*
 2814 *Astrophysical Journal*, 186, 97, doi: [10.1086/152480](https://doi.org/10.1086/152480)
- 2815 Dicke, R. H. 1964, *Nature*, 202, 432, doi: [10.1038/202432a0](https://doi.org/10.1038/202432a0)
- 2816 Disney, M. J. 2000, *General Relativity and Gravitation*, 32,
 2817 1125, doi: [10.1023/A:1001981929727](https://doi.org/10.1023/A:1001981929727)
- 2818 Djorgovski, S., & Spinrad, H. 1981, *The Astrophysical*
 2819 *Journal*, 251, 417, doi: [10.1086/159478](https://doi.org/10.1086/159478)
- 2820 Ellis, G. F. R. 1984, *Annual Review of Astronomy and*
 2821 *Astrophysics*, 22, 157,
 2822 doi: [10.1146/annurev.aa.22.090184.001105](https://doi.org/10.1146/annurev.aa.22.090184.001105)
- 2823 Eötvös, R. V., Pekár, D., & Fekete, E. 1922, *Annalen der*
 2824 *Physik*, 373, 11, doi: [10.1002/andp.19223730903](https://doi.org/10.1002/andp.19223730903)
- 2825 Feynman, R. P. 1965, *Feynman lectures on physics. Volume*
 2826 *3: Quantum mechanics*
- 2827 Field, G. B., & Henry, R. C. 1964, *The Astrophysical*
 2828 *Journal*, 140, 1002, doi: [10.1086/148000](https://doi.org/10.1086/148000)
- 2829 Finoguenov, A., Briel, U. G., Henry, J. P., et al. 2004,
 2830 *Astronomy and Astrophysics*, 419, 47,
 2831 doi: [10.1051/0004-6361:20035765](https://doi.org/10.1051/0004-6361:20035765)
- 2832 Fixsen, D. J. 2009, *ApJ*, 707, 916,
 2833 doi: [10.1088/0004-637X/707/2/916](https://doi.org/10.1088/0004-637X/707/2/916)
- 2834 Fixsen, D. J., Cheng, E. S., Gales, J. M., et al. 1996, *The*
 2835 *Astrophysical Journal*, 473, 576, doi: [10.1086/178173](https://doi.org/10.1086/178173)
- 2836 Freedman, W. L., Madore, B. F., Gibson, B. K., et al. 2001,
 2837 *The Astrophysical Journal*, 553, 47, doi: [10.1086/320638](https://doi.org/10.1086/320638)
- 2838 Fukada, Y., Hayakawa, S., Ikeda, M., et al. 1975,
 2839 *Astrophysics and Space Science*, 32, L1,
 2840 doi: [10.1007/BF00646232](https://doi.org/10.1007/BF00646232)
- 2841 Giacconi, R., Gursky, H., Paolini, F. R., & Rossi, B. B.
 2842 1962, *Physics Review Letters*, 9, 439,
 2843 doi: [10.1103/PhysRevLett.9.439](https://doi.org/10.1103/PhysRevLett.9.439)
- 2844 Goldhaber, G., Boyle, B., Bunclark, P., et al. 1996, *Nuclear*
 2845 *Physics B Proceedings Supplements*, Vol. 51, 51, 123,
 2846 doi: [10.1016/S0920-5632\(96\)00493-8](https://doi.org/10.1016/S0920-5632(96)00493-8)
- 2847 Goldhaber, G., Groom, D. E., Kim, A., et al. 2001, *The*
 2848 *Astrophysical Journal*, 558, 359, doi: [10.1086/322460](https://doi.org/10.1086/322460)
- 2849 Gould, R. J., & Burbidge, G. R. 1963, *The Astrophysical*
 2850 *Journal*, 138, 969, doi: [10.1086/147698](https://doi.org/10.1086/147698)

- 2851 Gruber, D. E., Matteson, J. L., Peterson, L. E., & Jung,
2852 G. V. 1999, *The Astrophysical Journal*, 520, 124,
2853 doi: [10.1086/307450](https://doi.org/10.1086/307450)
- 2854 Grun, E., Kruger, H., Srama, R., et al. 1999, in
2855 AAS/Division for Planetary Sciences Meeting Abstracts
2856 #31, AAS/Division for Planetary Sciences Meeting
2857 Abstracts, 55.03
- 2858 Grun, E., Zook, H. A., Fechtig, H., & Giese, R. H. 1985,
2859 *Icarus*, 62, 244, doi: [10.1016/0019-1035\(85\)90121-6](https://doi.org/10.1016/0019-1035(85)90121-6)
- 2860 Gurvits, L. I., Kellermann, K. I., & Frey, S. 1999,
2861 *Astromomy and Astrophysics*, 342, 378.
2862 <https://arxiv.org/abs/astro-ph/9812018>
- 2863 Guy, J., Astier, P., Baumont, S., et al. 2007, *Astromomy
2864 and Astrophysics*, 466, 11,
2865 doi: [10.1051/0004-6361:20066930](https://doi.org/10.1051/0004-6361:20066930)
- 2866 Guy, J., Sullivan, M., Conley, A., et al. 2010, *Astromomy
2867 and Astrophysics*, 523, A7,
2868 doi: [10.1051/0004-6361/201014468](https://doi.org/10.1051/0004-6361/201014468)
- 2869 Havas, P. 1966, *American Journal of Physics*, 34, 753,
2870 doi: [10.1119/1.1973468](https://doi.org/10.1119/1.1973468)
- 2871 Hawkins, M. R. S. 2003, *MNRAS*, 344, 492,
2872 doi: [10.1046/j.1365-8711.2003.06828.x](https://doi.org/10.1046/j.1365-8711.2003.06828.x)
- 2873 —. 2010, *MNRAS*, 405, 1940,
2874 doi: [10.1111/j.1365-2966.2010.16581.x](https://doi.org/10.1111/j.1365-2966.2010.16581.x)
- 2875 Holt, S. S. 1992, *Annals of the New York Academy of
2876 Sciences*, 655, 263,
2877 doi: [10.1111/j.1749-6632.1992.tb17076.x](https://doi.org/10.1111/j.1749-6632.1992.tb17076.x)
- 2878 Hoyle, F. 1962, *Astronomy*.
- 2879 Hoyle, F., Burbidge, G., Narlikar, J. V., & Livio, M. 2000,
2880 *Physics Today*, 53, 71, doi: [10.1063/1.1341928](https://doi.org/10.1063/1.1341928)
- 2881 Hughes, J. P. 1989, *The Astrophysical Journal*, 337, 21,
2882 doi: [10.1086/167084](https://doi.org/10.1086/167084)
- 2883 Itoh, N., Sakamoto, T., Kusano, S., Nozawa, S., &
2884 Kohyama, Y. 2000, *The Astrophysical Journal
2885 Supplement Series*, 128, 125, doi: [10.1086/313375](https://doi.org/10.1086/313375)
- 2886 Jackson, J. D. 1975, *Classical electrodynamics*
- 2887 Jones, D., Scolnic, D., Riess, A., et al. 2018, in *American
2888 Astronomical Society Meeting Abstracts #231*, Vol. 231,
2889 308.06
- 2890 Jones, D. O., Rodney, S. A., Riess, A. G., et al. 2013, *The
2891 Astrophysical Journal*, 768, 166,
2892 doi: [10.1088/0004-637X/768/2/166](https://doi.org/10.1088/0004-637X/768/2/166)
- 2893 Joseph, R. 2010, *Journal of Cosmology*, 6, 1547
- 2894 Kaiser, N., Burgett, W., Chambers, K., et al. 2010, in
2895 *Ground-based and Airborne Telescopes III*, Vol. 7733,
2896 77330E, doi: [10.1117/12.859188](https://doi.org/10.1117/12.859188)
- 2897 Karoji, H., Nottale, L., & Vigier, J. P. 1976, *Astrophysics
2898 and Space Science*, 44, 229, doi: [10.1007/BF00650484](https://doi.org/10.1007/BF00650484)
- 2899 Kessler, R., Becker, A. C., Cinabro, D., et al. 2009a, *The
2900 Astrophysical Journal Supplement Series*, 185, 32,
2901 doi: [10.1088/0067-0049/185/1/32](https://doi.org/10.1088/0067-0049/185/1/32)
- 2902 Kessler, R., Bernstein, J. P., Cinabro, D., et al. 2009b,
2903 *Publications of the Astronomical Society of the Pacific*,
2904 121, 1028, doi: [10.1086/605984](https://doi.org/10.1086/605984)
- 2905 Kinzer, R. L., Jung, G. V., Gruber, D. E., et al. 1997, *The
2906 Astrophysical Journal*, 475, 361, doi: [10.1086/303507](https://doi.org/10.1086/303507)
- 2907 Kormendy, J. 1977, *The Astrophysical Journal*, 218, 333,
2908 doi: [10.1086/155687](https://doi.org/10.1086/155687)
- 2909 Kowalski, M., Rubin, D., Aldering, G., et al. 2008, *The
2910 Astrophysical Journal*, 686, 749, doi: [10.1086/589937](https://doi.org/10.1086/589937)
- 2911 Lal, A. K. 2010, *Journal of Cosmology*, 6, 1533
- 2912 Le Sergeant D'Hendecourt, L. B., & Lamy, P. L. 1980,
2913 *Icarus*, 43, 350, doi: [10.1016/0019-1035\(80\)90180-3](https://doi.org/10.1016/0019-1035(80)90180-3)
- 2914 Lerner, E. J. 1991, *The big bang never happened*
- 2915 Lieu, R., Mittaz, J. P. D., & Zhang, S.-N. 2006, *The
2916 Astrophysical Journal*, 648, 176, doi: [10.1086/505627](https://doi.org/10.1086/505627)
- 2917 Liu, M. C., & Graham, J. R. 2001, *The Astrophysical
2918 Journal*, 557, L31, doi: [10.1086/323174](https://doi.org/10.1086/323174)
- 2919 Longair, M. S. 1991, *Astronomy*, 19, 95
- 2920 López-Corredoira, M. 2010, *International Journal of
2921 Modern Physics D*, 19, 245,
2922 doi: [10.1142/S0218271810016397](https://doi.org/10.1142/S0218271810016397)
- 2923 Lubin, L. M., & Sandage, A. 2001a, *The Astronomical
2924 Journal*, 121, 2289, doi: [10.1086/320401](https://doi.org/10.1086/320401)
- 2925 —. 2001b, *The Astronomical Journal*, 122, 1071,
2926 doi: [10.1086/322133](https://doi.org/10.1086/322133)
- 2927 —. 2001c, *The Astronomical Journal*, 122, 1084,
2928 doi: [10.1086/322134](https://doi.org/10.1086/322134)
- 2929 Lyke, B. W., Higley, A. N., McLane, J. N., et al. 2020, *The
2930 Astrophysical Journal Supplement Series*, 250, 8,
2931 doi: [10.3847/1538-4365/aba623](https://doi.org/10.3847/1538-4365/aba623)
- 2932 Mandrou, P., Vedrenne, G., & Niel, M. 1979, *The
2933 Astrophysical Journal*, 230, 97, doi: [10.1086/157065](https://doi.org/10.1086/157065)
- 2934 Marshall, F. E., Boldt, E. A., Holt, S. S., et al. 1980, *The
2935 Astrophysical Journal*, 235, 4, doi: [10.1086/157601](https://doi.org/10.1086/157601)
- 2936 Mather, J. C., Cheng, E. S., Eplee, R. E., J., et al. 1990,
2937 *The Astrophysical Journal*, 354, L37, doi: [10.1086/185717](https://doi.org/10.1086/185717)
- 2938 Mayall, N. U. 1960, *Annales d'Astrophysique*, 23, 344
- 2939 Mazets, E. P., Golenetskii, S. V., Ilinskii, V. N., Gurian,
2940 I. A., & Kharitonova, T. V. 1975, *Astrophysics and Space
2941 Science*, 33, 347, doi: [10.1007/BF00640104](https://doi.org/10.1007/BF00640104)
- 2942 Misner, C. W., Thorne, K. S., & Wheeler, J. A. 1973,
2943 *Gravitation*
- 2944 Nottale, L. 1976, *The Astrophysical Journal*, 208, L103,
2945 doi: [10.1086/182242](https://doi.org/10.1086/182242)
- 2946 Nottale, L., & Vigier, J. P. 1977, *Nature*, 268, 608,
2947 doi: [10.1038/268608a0](https://doi.org/10.1038/268608a0)

- 2948 Nozawa, S., Itoh, N., & Kohyama, Y. 1998, The
2949 Astrophysical Journal, 507, 530, doi: [10.1086/306352](https://doi.org/10.1086/306352)
- 2950 Peebles, P. J. E. 1993, Principles of Physical Cosmology
- 2951 Petrosian, V. 1976, The Astrophysical Journal, 210, L53,
2952 doi: [10.1086/182301](https://doi.org/10.1086/182301)
- 2953 Pettini, M., Hunstead, R. W., Smith, L. J., & Mar, D. P.
2954 1990, Monthly Notices of the Royal Astronomical
2955 Society, 246, 545
- 2956 Phillips, M. M. 1993, The Astrophysical Journal Letters,
2957 413, L105, doi: [10.1086/186970](https://doi.org/10.1086/186970)
- 2958 Pimblet, K. A. 2003, Publications of the Astronomical
2959 Society of Australia, 20, 294, doi: [10.1071/AS03043](https://doi.org/10.1071/AS03043)
- 2960 Postman, M., & Lauer, T. R. 1995, The Astrophysical
2961 Journal, 440, 28, doi: [10.1086/175245](https://doi.org/10.1086/175245)
- 2962 Pound, R. V., & Snider, J. L. 1965, Physical Review, 140,
2963 788, doi: [10.1103/PhysRev.140.B788](https://doi.org/10.1103/PhysRev.140.B788)
- 2964 Ratcliffe, H. 2010, Journal of Cosmology, 4, 693
- 2965 Rauch, M. 1998, Annual Review of Astronomy and
2966 Astrophysics, 36, 267,
2967 doi: [10.1146/annurev.astro.36.1.267](https://doi.org/10.1146/annurev.astro.36.1.267)
- 2968 Raychaudhuri, A. 1955, Physical Review, 98, 1123,
2969 doi: [10.1103/PhysRev.98.1123](https://doi.org/10.1103/PhysRev.98.1123)
- 2970 Riess, A. G., Strolger, L.-G., Casertano, S., et al. 2007, The
2971 Astrophysical Journal, 659, 98, doi: [10.1086/510378](https://doi.org/10.1086/510378)
- 2972 Rood, H. J. 1988, Annual Review of Astronomy and
2973 Astrophysics, 26, 245,
2974 doi: [10.1146/annurev.aa.26.090188.001333](https://doi.org/10.1146/annurev.aa.26.090188.001333)
- 2975 Rood, H. J., & Struble, M. F. 1982, The Astrophysical
2976 Journal, 252, L7, doi: [10.1086/183708](https://doi.org/10.1086/183708)
- 2977 Roth, K. C., & Meyer, D. M. 1995, The Astrophysical
2978 Journal, 441, 129, doi: [10.1086/175343](https://doi.org/10.1086/175343)
- 2979 Sandage, A. 2010, The Astronomical Journal, 139, 728,
2980 doi: [10.1088/0004-6256/139/2/728](https://doi.org/10.1088/0004-6256/139/2/728)
- 2981 Sandage, A., & Lubin, L. M. 2001, The Astronomical
2982 Journal, 121, 2271, doi: [10.1086/320394](https://doi.org/10.1086/320394)
- 2983 Sandage, A., & Perlmutter, J.-M. 1990, The Astrophysical
2984 Journal, 361, 1, doi: [10.1086/169161](https://doi.org/10.1086/169161)
- 2985 Santangelo, N., Horstman, H., & Horstman-Moretti, E.
2986 1973, SoPh, 29, 143, doi: [10.1007/BF00153445](https://doi.org/10.1007/BF00153445)
- 2987 Scolnic, D. M., Jones, D. O., Rest, A., et al. 2017, ArXiv
2988 e-prints. <https://arxiv.org/abs/1710.00845>
- 2989 —. 2018, The Astrophysical Journal, 859, 101,
2990 doi: [10.3847/1538-4357/aab9bb](https://doi.org/10.3847/1538-4357/aab9bb)
- 2991 Sunyaev, R. A., & Zeldovich, I. B. 1980, Monthly Notices of
2992 the Royal Astronomical Society, 190, 413,
2993 doi: [10.1093/mnras/190.3.413](https://doi.org/10.1093/mnras/190.3.413)
- 2994 Sunyaev, R. A., & Zeldovich, Y. B. 1970, Astrophysics and
2995 Space Science, 9, 353, doi: [10.1007/BF00649576](https://doi.org/10.1007/BF00649576)
- 2996 Tolman, R. C. 1934, Relativity, Thermodynamics, and
2997 Cosmology
- 2998 Trombka, J. I., Dyer, C. S., Evans, L. G., et al. 1977, The
2999 Astrophysical Journal, 212, 925, doi: [10.1086/155117](https://doi.org/10.1086/155117)
- 3000 van Flandern, T. 1991, in Bulletin of the American
3001 Astronomical Society, Vol. 23, 1395
- 3002 Watt, M. P., Ponman, T. J., Bertram, D., et al. 1992,
3003 Monthly Notices of the Royal Astronomical Society, 258,
3004 738, doi: [10.1093/mnras/258.4.738](https://doi.org/10.1093/mnras/258.4.738)
- 3005 White, S. D. M., Briel, U. G., & Henry, J. P. 1993,
3006 Monthly Notices of the Royal Astronomical Society, 261,
3007 L8, doi: [10.1093/mnras/261.1.L8](https://doi.org/10.1093/mnras/261.1.L8)
- 3008 Wolf, C., Wisotzki, L., Borch, A., et al. 2003, Astromomy
3009 and Astrophysics, 408, 499,
3010 doi: [10.1051/0004-6361:20030990](https://doi.org/10.1051/0004-6361:20030990)
- 3011 Wolf, C., Meisenheimer, K., Kleinheinrich, M., et al. 2004,
3012 Astromomy and Astrophysics, 421, 913,
3013 doi: [10.1051/0004-6361:20040525](https://doi.org/10.1051/0004-6361:20040525)
- 3014 Wood-Vasey, W. M., Friedman, A. S., Bloom, J. S., et al.
3015 2008, The Astrophysical Journal, 689, 377,
3016 doi: [10.1086/592374](https://doi.org/10.1086/592374)
- 3017 Zwicky, F. 1937, The Astrophysical Journal, 86, 217,
3018 doi: [10.1086/143864](https://doi.org/10.1086/143864)